Available online at www.sciencedirect.com
SCIENCE DIRECT®
Journal of Computational Physics 197 (2004) 387–417
JOURNAL OF COMPUTATIONAL PHYSICS
www.elsevier.com/locate/jcp

Multiphase semiclassical approximation of an electron in a one-dimensional crystalline lattice ☆ I. Homogeneous problems

Laurent Gosse [a,*], Peter A. Markowich [b]

[a] *IAC-CNR "Mauro Picone" (sezione di Bari), Via Amendola 122/I-70126 Bari, Italy*
[b] *Institüt für Mathematik, University of Vienna, Boltzmanngasse, 9-A-1090 Vienna, Austria*

Received 16 April 2003; received in revised form 4 December 2003; accepted 4 December 2003
Available online 23 January 2004

Abstract

We present a computational approach for the WKB approximation of the wave function of an electron moving in a periodic one-dimensional crystal lattice. We derive a nonstrictly hyperbolic system for the phase and the intensity where the flux functions originate from the Bloch spectrum of the Schrödinger operator. Relying on the framework of the multibranch entropy solutions introduced by Brenier and Corrias, we compute efficiently multiphase solutions using well adapted and simple numerical schemes. In this first part we present computational results for vanishing exterior potentials which demonstrate the effectiveness of the proposed method.

AMS: 81Q05; 81Q20; 35L65; 65M06

Keywords: Semiclassical limit; Periodic potential; Homogenization; Vlasov equation; Moment method; Non-strictly hyperbolic systems

1. Introduction

This article is the first part of a numerical study of semiclassical approximation of the motion of electrons in short-scale periodic potentials. This phenomenon is quantum mechanical and we shall represent particles as wave packets with localized wave numbers κ. Then if such a wave packet spreads over many

☆ Both authors were partially supported by the EEC network #HPRN-CT-2002-00282, the "Modelling and Computations in Wave Propagation" contract #HPMD-CT-2001-00121 and the Wittgenstein 2000 Award of P.A. Markowich funded by the Austrian Research Fund FWF. Also support from the Austrian FWF Project P14876 No. 4 is acknowledged.
* Corresponding author.
E-mail addresses: l.gosse@area.ba.cnr.it (L. Gosse), Peter.Markowich@univie.ac.at (P.A. Markowich).

0021-9991/$ - see front matter
doi:10.1016/j.jcp.2003.12.004

lattice periods, the wave number can be considered constant and the dynamics are ruled by the energy bands. This is of common use in solid-state physics [2].

More precisely, we start from the Schrödinger equation in one space dimension

$$\mathrm{i}\hbar\partial_t\psi + \frac{\hbar^2}{2m}\partial_{xx}\psi = eV(x)\psi, \quad x \in \mathbb{R} \tag{1}$$

with $\hbar$ is the Planck constant, m and e are the electronic mass and charge and $V \in \mathbb{R}$ is the periodic potential modelling the interaction with a lattice of ionic cores in one space dimension ($x \in \mathbb{R}$). We first change to "atomic units" for which $\hbar = m = e = 1$. Then we introduce the dimensionless parameter ε as the microscopic–macroscopic ratio; we assume it small and track wave packets with a spatial spreading of the order of $1/\varepsilon$. We recast (1) in macroscopic variables $x \mapsto x/\varepsilon$, $t \mapsto t/\varepsilon$ (i.e. we study $O(\varepsilon)$-wavelength solutions) and a scaled problem arises

$$\mathrm{i}\varepsilon\partial_t\psi + \frac{\varepsilon^2}{2}\partial_{xx}\psi = V\left(\frac{x}{\varepsilon}\right)\psi, \quad V(x+2\pi) = V(x) \tag{2}$$

for which the limit $\varepsilon \to 0$ is of special interest. We assumed the period to be 2π on the atomic lengthscale for the sake of simplicity only.

From the mathematical point of view, the asymptotics of (2) correspond to a combined semiclassical and homogenization limit. Rigorous theorems in this direction have been proven in the last decade by the authors of [4,27,42,46,49]. Wigner transforms of the wave function ψ were extensively used ($\bar{\cdot}$ stands for complex conjugation)

$$W(t,x,\xi) = \int_{\mathbb{R}} \psi\left(t, x + \frac{\varepsilon y}{2}\right)\bar{\psi}\left(t, x - \frac{\varepsilon y}{2}\right)\exp(\mathrm{i}\xi y)\,\mathrm{d}y. \quad \xi \in \mathbb{R}.$$

In fact, in order to take full advantage of the periodic structure of (1), the right object has been found to be the so-called Wigner series which reads

$$w(t,x,\kappa) = \sum_{j\in\mathbb{Z}} \psi(t, x + \varepsilon j\pi)\bar{\psi}(t, x - \varepsilon j\pi)\exp(-2\pi\mathrm{i}\kappa j), \quad \kappa \in B \tag{3}$$

and from which one can deduce for instance the electron's position density

$$\rho(t,x) = \int_B w(t,x,\kappa)\frac{\mathrm{d}\kappa}{|B|}, \quad B \text{ the first Brillouin zone.}$$

A summary of these results will be presented in Section 2.3. Before going further, some classical definitions are recalled in order to facilitate the understanding of this paper in terms of the existing literature:

- The Bravais lattice for (1) and (2) is $\Gamma = 2\pi\mathbb{Z}$; its primitive cell is $]0, 2\pi[$.
- The reciprocal lattice Γ' is the set of wave numbers κ for which plane waves $\exp(\mathrm{i}\kappa x)$ have the same periodicity as the potential V; i.e. $\Gamma' = \mathbb{Z}$.
- The first Brillouin zone B is the Wigner–Seitz cell of the dual lattice Γ' made of all κ closer to zero than to any other dual lattice point; $B =]-\frac{1}{2}, \frac{1}{2}[$.

Then, by means of (3), one passes from (2) as $\varepsilon \to 0$ to a kinetic equation for a density $f \simeq w$ which is solution of the transport equation

$$\partial_t f(t,x,\kappa) + E_n'(\kappa)\partial_x f(t,x,\kappa) = 0, \quad f \geqslant 0. \tag{4}$$

The set of all functions $E_n(\kappa)$ corresponds to the band structure of (2) whose derivation will be presented in detail in Section 2.2. From these considerations, one could deduce that this "Wigner approach" also

indicates an appropriate route towards computational algorithms. Indeed, upon taking κ-moments of (4), a system of conservation laws can be written when assuming that $f(t,x,\kappa)=\sum_\ell \rho_\ell(t,x)\delta(\kappa-p_\ell(t,x))$, which means that particles of mass/velocity ρ_ℓ/p_ℓ are tracked in phase space while moving according to the Hamiltonian $E_n(p)$. However, these weakly hyperbolic systems turn out to be rather delicate to simulate [23,36,48] since even for the simplest case $\ell\equiv 1$ (the so-called monokinetic density), one faces the pressureless gas problem admitting measure-valued solutions; see [10,15] and references therein.

An alternative strategy can be proposed relying on classical WKB expansions, see [38] and the original references in [17]. Considerations of this nature usually lead to simpler systems made of a Hamilton–Jacobi equation for the phase of the wave function coupled to a continuity equation for its intensity. However, at this level, the difficulty lies more in finding a way to elicit a correct solution: clearly the framework of viscosity solutions [22,26,31] does not fit since the entropy conditions destroy the folds generally appearing in phase space. It has been recently shown that when the number of these folds is finite, there exists a way to reconstruct exactly the "geometric solution" [13,35] by solving a much less singular moments system. Roughly speaking, it consists in solving (4) with the smoother kinetic density $f(t,x,\kappa)=\sum_\ell(-1)^{\ell-1}H(p_\ell(t,x)-\kappa)$, H is the Heaviside function, following [14] as will be developed in Section 3.1 (the cases $\ell=1,2$ have been treated in [13,43,44]); this technique has already been investigated numerically in [30,32,48]. For other methods, we refer the reader to [6,16,23,37,50]. We stress that, besides a possibly lower computational cost, a semiclassical simulation presents advantages when compared to a direct simulation of the wave function satisfying (1): it naturally reveals the band and caustic structures.

When carrying out the WKB asymptotics in Section 2.1 in the spirit of [33], an essential point lies in computing efficiently the Bloch spectrum of the Hamiltonian operator $\mathscr{H}(x,\mathrm{i}\partial_x)=-(1/2)\partial_{xx}+V(x)$. This constitutes one of the main numerical difficulties as it amounts to solving an eigenvalue problem for a Sturm–Liouville equation [53]. We propose in Section 2.2 a way around it avoiding semiclassical quantization [18,21,38] but using spectral techniques. Finally, Sections 4 and 5 are devoted to the study of practical examples including the Mathieu's equation and the Kronig–Penney model [40]. Numerical computations making use of the so-called parabolic band approximation [2,47] for moderate wave numbers and a Fourier representation of the bands when considering the whole Brillouin zone are presented. The most classical approach is of course ray-tracing in phase space; however, its accuracy can sometimes be really low when compared to Eulerian methods [6,50]. We also present preliminary numerical comparisons between a direct Fourier simulation of (2) and a multiphase WKB approximation relying on the aforementioned K-branch solutions. In Appendix A, we comment on the connection with effective Hamiltonians obtained when homogenizing Hamilton–Jacobi equations in the sense of [19,20,41].

We close this introduction mentioning that in a forthcoming paper (Part II of this work), we shall report on computations with nontrivial exterior potentials; that is to say, approximation for small values of ε of

$$\mathrm{i}\varepsilon\partial_t\psi+\frac{\varepsilon^2}{2}\partial_{xx}\psi=\left(V\left(\frac{x}{\varepsilon}\right)+V_e(x)\right)\psi, \tag{5}$$

instead of (2) in case $V_e\in\mathbb{R}$ is smooth. A concrete example is Coulomb interaction; first considerations on this more delicate problem are stated in Section 6.

2. The WKB method in one space dimension

We are concerned with highly oscillating wave-packet solutions of the Cauchy problem for the following one-dimensional Schrödinger equation:

$$\mathrm{i}\varepsilon\partial_t\psi+\frac{\varepsilon^2}{2}\partial_{xx}\psi=\left(V\left(\frac{x}{\varepsilon}\right)+V_e(x)\right)\psi,\quad \varepsilon\to 0, \tag{6}$$

where V is 2π-periodic and V_e is smooth. Generally, one is tempted to describe these solutions by means of plane waves of the form $\psi(t,x) = A(t,x)\exp(\mathrm{i}\varphi(t,x)/\varepsilon)$ for A and φ being possibly multivalued; plugging this ansatz into (6) leads to a relation between the wave's phase φ and its amplitude A:

$$-A\left(\partial_t\varphi + \frac{(\partial_x\varphi)^2}{2} + V\left(\frac{x}{\varepsilon}\right) + V_e(x)\right) + \frac{\mathrm{i}\varepsilon}{2}(2\partial_t A + A\partial_{xx}\varphi + 2\partial_x A\,\partial_x\varphi) + \frac{\varepsilon^2}{2}\partial_{xx}A = 0.$$

Splitting this equation into real and imaginary parts yields

$$\partial_t\varphi + \frac{(\partial_x\varphi)^2}{2} + V\left(\frac{x}{\varepsilon}\right) + V_e(x) = \frac{\varepsilon^2}{2A}\partial_{xx}A, \quad \partial_t(A^2) + \partial_x(A^2\,\partial_x\varphi) = 0. \tag{7}$$

Moreover, neglecting the term $\varepsilon^2\partial_{xx}A/2A$ leads to the weakly coupled system

$$\partial_t\varphi + \frac{(\partial_x\varphi)^2}{2} + V\left(\frac{x}{\varepsilon}\right) + V_e(x) = 0, \quad \partial_t(A^2) + \partial_x(A^2\,\partial_x\varphi) = 0. \tag{8}$$

The phase φ evolves according to a nonlinear Hamilton–Jacobi equation whose Hamiltonian $\mathscr{H}(x,x/\varepsilon,p) = p^2/2 + V(x/\varepsilon) + V_e(x)$ contains a fine-scale term. The intensity of the plane wave $|\psi|^2 = A^2$ evolves in time according to a linear conservation law whose velocity field is given by the x-derivative of φ. Still, this system needs to be homogenized in order to describe the limit behaviour as $\varepsilon \to 0$ of (6); such a theory exists up to now only in the context of viscosity solutions (see [19,20,24,25,41] and Appendix A of this paper) which does not fully describe the dispersive structure of (7).

2.1. WKB expansion and emergence of the Bloch spectrum

As we just saw, the naive ansatz does not have the correct structure as it leads to a system in which the small parameter ε remains present. Hence following [7,33], a refinement can be proposed considering a two-scale amplitude

$$A\left(t,x,y = \frac{x}{\varepsilon}\right) = A_0(t,x,y) + \varepsilon A_1(t,x,y) + \cdots; \quad A(t,x,y+2\pi) = A(t,x,y). \tag{9}$$

Taking this new dependence into account inside (6) yields the expression

$$\begin{aligned} &-A\partial_t\varphi + \frac{1}{2}\left(\partial_{yy}A - A(\partial_x\varphi)^2 + 2\mathrm{i}(\partial_x\varphi)(\partial_y A)\right) - (V(y) + V_e(x))A \\ &\quad + \frac{\mathrm{i}\varepsilon}{2}\left(2\partial_t A + A\partial_{xx}\varphi + 2\partial_x A\,\partial_x\varphi - 2\mathrm{i}\partial_{xy}A\right) + \frac{\varepsilon^2}{2}\partial_{xx}A = 0. \end{aligned} \tag{10}$$

- The first step is to compare the O(1) terms; this concerns A_0

$$\frac{1}{2}\partial_{yy}A_0 - V(y)A_0 + \left(\mathrm{i}(\partial_x\varphi)(\partial_y A_0) - \frac{1}{2}A_0(\partial_x\varphi)^2\right) = A_0(\partial_t\varphi + V_e(x)).$$

As we shall see below, this means that $\partial_t\varphi + V_e$ has to be an eigenvalue associated to the eigenfunction A_0 for a certain time-independent Schrödinger operator. Indeed, let us consider the quantum mechanical momentum operator $\hat{p} = \mathrm{i}\partial_y$ and look at the eigenmodes of $\mathscr{H}(y,\hat{p}) = -(1/2)\partial_{yy} + V(y)$ written in the Bloch-wave form $\Psi_\kappa(y) = \exp(\mathrm{i}\kappa y)z_\kappa(y)$ for some real wave-number κ and a 2π-periodic modulation z_κ (see Theorem 1). Then if Ψ_κ satisfies

$$\forall y \in \mathbb{R}, \quad \mathscr{H}(y,\hat{p})\Psi_\kappa = -\frac{1}{2}\partial_{yy}\Psi_\kappa + V(y)\Psi_\kappa = E(\kappa)\Psi_\kappa \tag{11}$$

for $E : \mathbb{R} \to \mathbb{R}$ being 1-periodic, then it easily follows that the envelope z_κ solves

$$-\frac{1}{2}\partial_{yy}z_\kappa + V(y)z_\kappa - \left(\mathrm{i}\kappa\partial_y z_\kappa - \frac{\kappa^2}{2}z_\kappa\right) = E(\kappa)z_\kappa.$$

Thus O(1) terms inside (10) cancel if and only if $y \mapsto A_0(t,x,y)\exp(\mathrm{i}\kappa y)$ is an eigenstate of $\mathscr{H}(y,\hat{p})$ associated to the eigenvalue $E(\partial_x\varphi) = -\partial_t\varphi - V_e(x)$

$$\mathscr{H}(y,\hat{p})(A_0\exp(\mathrm{i}\kappa y)) = -(\partial_t\varphi + V_e(x))(A_0\exp(\mathrm{i}\kappa y)), \quad \kappa = \partial_x\varphi.$$

Note that the slow variable x shows up only as a parameter. Written in a more compact form, an Hamilton–Jacobi equation has been derived, where the fine scale $y = x/\varepsilon$ has disappeared

$$\partial_t\varphi + E(\partial_x\varphi) + V_e(x) = 0. \tag{12}$$

- The second step consists in writing $A_0(t,x,y) = a_0(t,x)z_\kappa(y)$ with stationary orthonormal modulations: $\|z_\kappa\|_{L^2(0,2\pi)} = 1$. Hence comparing $\mathrm{O}(\varepsilon)$ terms inside (10) taking into account (9) has been shown in [33] to be equivalent to the linear conservation law

$$\partial_t(a_0)^2 + \partial_x\Big((a_0)^2 E'(\partial_x\varphi)\Big) = 0. \tag{13}$$

All in all, starting from the Schrödinger equation (6), one has to consider the Bloch spectral decomposition (11) producing a countable set of distorted plane waves Ψ_κ^n, $n \in \mathbb{N}$, associated to the energy bands $E_n(\kappa)$. Then a convenient nth band ansatz reads

$$\tilde{\psi}_n^\varepsilon(t,x) = a_n(t,x)\exp\left(\frac{\mathrm{i}\varphi(t,x)}{\varepsilon}\right) z_\kappa^n(x/\varepsilon), \quad \kappa = \partial_x\varphi(t,x), \tag{14}$$

where the unknowns evolve according to the nth band WKB system (12), (13)

$$\partial_t\varphi + E_n(\partial_x\varphi) + V_e(x) = 0, \quad \partial_t\mu + \partial_x\big(E_n'(\partial_x\varphi)\ \mu\big) = 0, \quad \mu = (a_n)^2. \tag{15}$$

So $|\tilde{\psi}_n^\varepsilon|^2 = \mu|z^n_{\partial_x\varphi}|^2$ and the WKB expansion is used for the transient computation of a plane wave, the modulation z_κ evolving only through the relation $\kappa = \partial_x\varphi$. In [33], it has been argued that $\tilde{\psi}_n^\varepsilon$ provides an $\mathrm{O}(\varepsilon)$-approximation of the solution of the Schrödinger equation (6) with identical initial datum before caustic onset, i.e. as long as (15) admits a smooth solution. In the next subsection, we shall focus on the Bloch wave decomposition from both theoretical and computational points of view. Note that system (15) can recover the exact solution of (1) in case the dispersive term in (7) is zero. This happens for nth band wavepackets which read like

$$\psi^\varepsilon(x) = \int_B \exp(\mathrm{i}\kappa x/\varepsilon)z_\kappa^n(x/\varepsilon)\,\mathrm{d}\kappa$$

for which $a_0 \equiv 1$.

In the special case $V_e \equiv 0$ and $\psi^\varepsilon(t=0,x) = \int_B \sigma(\kappa)\exp(\mathrm{i}\kappa x/\varepsilon)z_\kappa^n(x/\varepsilon)\,\mathrm{d}\kappa = \int_B \sigma(\kappa)\Psi_\kappa^n(x/\varepsilon)\,\mathrm{d}\kappa$, both (15) and (1) furnish $\psi^\varepsilon(t,x) = \int_B \sigma(\kappa)\exp(\mathrm{i}(\kappa x - E_n(\kappa)t)/\varepsilon)z_\kappa^n(x/\varepsilon)\,\mathrm{d}\kappa$.

2.2. Derivation of the Sturm–Liouville eigenmodes

We begin by recalling the:

Theorem 1 (Bloch's theorem, [8]). *Let the potential V be 2π-periodic. Then each eigenstate Ψ of $\mathscr{H}(y,\hat{p}) = -(1/2)\partial_{yy} + V(y)$ satisfies $\Psi(y+2\pi) = \exp(2i\kappa\pi)\Psi(y)$ for all $y \in \mathbb{R}$ and some value $\kappa \in [-\frac{1}{2},\frac{1}{2}]$.*

Its proof is based on the fact that $\mathscr{H}$ commutes with the y-translation operator $\tau_{\pm 2\pi}$; thus any eigenstate of $\mathscr{H}$ is also one of $\tau_{\pm 2\pi}$ for some complex eigenvalue. An important role is played by functions having phase-shifts when translated of 2π.

Definition 1 (*κ-quasiperiodic functions*). Any function $\Psi \in C^0(\mathbb{R})$ satisfying $\Psi(y+2\pi) = \exp(2i\kappa\pi)\Psi(y)$ for all $y \in \mathbb{R}$ is called a κ-quasiperiodic function.

Obviously a 0-quasiperiodic function is 2π-periodic. There are decomposition and synthesis relations for functions of this kind in $L^2(\mathbb{R})$, see [27,46] for instance. We now define $\mathscr{H}_\kappa$ as the steady operator $\mathscr{H}$ restricted to κ-quasiperiodic functions for some $\kappa \in B$. Its spectral structure is well known, see e.g. [46]; one has to find all the pairs $\{E_n(\kappa), \Psi^n_\kappa;\ \kappa \in]-\frac{1}{2},\frac{1}{2}[\}$ for $n \in \mathbb{N}$ satisfying

$$\forall y \in \mathbb{R}, \quad \begin{cases} -\frac{1}{2}\partial_{yy}\Psi^n_\kappa + V(y)\Psi^n_\kappa = E_n(\kappa)\Psi^n_\kappa, \\ \Psi^n_\kappa \text{ and } \partial_y\Psi^n_\kappa \text{ are } \kappa\text{-quasiperiodic.} \end{cases} \tag{16}$$

For any fixed $\kappa \in B$, there exists a complete set of eigenfunctions Ψ^n_κ orthonormal in $L^2(0,2\pi)$ with countably many eigenvalues $E_1(\kappa) < E_2(\kappa) < \cdots < E_{n-1}(\kappa) < E_n(\kappa) < \cdots$. The set $\{E_n(\kappa);\ \kappa \in]-\frac{1}{2},\frac{1}{2}[\}$ is called the nth energy band of $\mathscr{H}$ whereas Ψ^n_κ is a nth Bloch function (or Bloch state). We also have for all κ, $E_n(\kappa) \to +\infty$ as $n \to +\infty$ and each map $\kappa \mapsto E_n(\kappa)$ is extended 1-periodically. The Bloch states Ψ^n_κ have the form already encountered in Section 2.1: $\Psi^n_\kappa(x) = \exp(i\kappa x)z^n_\kappa(x)$ for a certain 2π-periodic modulation. Now we notice that a scaling argument gives straightforwardly

$$\mathscr{H}(y,\hat{p})\Psi^n_\kappa(y) = E_n(\kappa)\Psi^n_\kappa(y) \iff \mathscr{H}(x/\varepsilon, \varepsilon\hat{p})\Psi^n_\kappa(x/\varepsilon) = E_n(\kappa)\Psi^n_\kappa(x/\varepsilon).$$

Moreover, $\Psi^n_\kappa(\cdot/\varepsilon)/\sqrt{\varepsilon}$ is still orthonormal in $L^2(0,2\varepsilon\pi)$.

In order to carry out the WKB program outlined in Section 2.1, an important stepping stone is the Bloch decomposition of $\mathscr{H}$ for all $\kappa \in B$. There exists several methods to do so: among them, one consists in solving directly the Sturm–Liouville problem (16), see [53], while another one relies on semiclassical quantization rules following [21,38] (see also [18]). We turn to a spectral approach, taking advantage of the free package SciLab (available at http://www-rocq.inria.fr/scilab) as in [39]. We consider for now the potential $V \in C^1_{\text{per}}(\mathbb{R})$ and expand it in its Fourier series:

$$V(y) = \sum_{q\in\mathbb{Z}} \hat{V}_q \exp(iqy), \quad \hat{V}_q = \frac{1}{2\pi}\int_0^{2\pi} V(y)\exp(-iqy)\,dy. \tag{17}$$

Since $\Psi^n_\kappa(y) = \exp(i\kappa y)z^n_\kappa(y)$ with $z^n_\kappa(y+2\pi) = z^n_\kappa(y)$, any Bloch state can also be expanded in plane waves written in Dirac's notation:

$$\forall (q,\kappa) \in \mathbb{Z} \times \left[-\frac{1}{2},\frac{1}{2}\right], \quad |q,\kappa\rangle = \exp(i(q+\kappa)y).$$

Hence we have in mind to approximate the differential Sturm–Liouville equation (16) by an eigenvalue problem for the matrix H_κ defined as follows with $N \in \mathbb{N}$:

$$H_\kappa = \left(\langle q',\kappa|\mathscr{H}_\kappa|q,\kappa\rangle\right)_{q,q'}, \quad \kappa \in \left[-\frac{1}{2},\frac{1}{2}\right], \quad q,q' \in \{-N,\ldots,N\}.$$

The kinetic energy entries are easily calculated as

$$-\frac{1}{2\pi}\int_0^{2\pi}\exp(-\mathrm{i}(q+\kappa)y)\frac{1}{2}\partial_{yy}\exp(\mathrm{i}(q'+\kappa)y)\,\mathrm{d}y=\frac{1}{2}(q+\kappa)(q'+\kappa)\delta_{q,q'}$$

with $\delta_{q,q'}$ is the classical Christoffel symbol. The potential is to be treated the same way and using its Fourier coefficients, one finds easily a Toeplitz representation

$$\langle q',\kappa|V(y)|q,\kappa\rangle=\frac{1}{2\pi}\int_0^{2\pi}V(y)\exp(-\mathrm{i}(q-q')y)\,\mathrm{d}y=\hat{V}_{q-q'},$$

which in turn leads to an eigenvalue problem for the following matrix:

$$H_\kappa=\begin{pmatrix}\hat{V}_0+\frac{1}{2}(\kappa-N)^2 & \hat{V}_{-1} & \cdots & \hat{V}_{-2N}\\ \hat{V}_1 & \hat{V}_0+\frac{1}{2}(\kappa-N+1)^2 & & \vdots\\ \vdots & & \ddots & \hat{V}_{-1}\\ \hat{V}_{2N} & \cdots & \hat{V}_1 & \hat{V}_0+\frac{1}{2}(\kappa+N)^2\end{pmatrix}. \tag{18}$$

We notice that since $V(x)\in\mathbb{R}$, $\hat{V}_{-q}=\bar{\hat{V}}_q$ and H_κ is Hermitian. If V is even, it is real symmetric and optimized algorithms can be used. The eigenvalues and their corresponding eigenvectors for H_κ are approximations of the energy bands $E_n(\kappa)$ and the Fourier coefficients (with indices $-N,\ldots,0,1,\ldots,N$) of the modulations $z_\kappa^n(y)$.

A simple and important case is the so-called Mathieu's equation corresponding to (16) with $V(x)=\cos(x)$; all the $\hat{V}_q$'s are zero except $\hat{V}_{\pm1}=1/2$. The outcoming matrix H_κ is tridiagonal symmetric for all $\kappa\in B$. This technique applies also to the so-called Kronig–Penney's model [40] with discontinuous potential

$$V(y)=1-\sum_{j\in\mathbb{Z}}\mathbf{1}_{y\in[\frac{\pi}{2}+2j\pi,\frac{3\pi}{2}+2j\pi]}, \tag{19}$$

and $\mathbf{1}_A$ stands for the characteristic function of a set A. The lattice atoms are meant to be in the potential wells located around $\pi(1+2\mathbb{Z})$. Its corresponding Fourier coefficients are

$$\hat{V}_0=\frac{1}{2},\quad \hat{V}_q=\frac{\sin(q\pi/2)}{q\pi}.$$

In this case, the H_κ matrix is still real symmetric but full since all frequencies are present (however, harmonics decay like $\mathrm{O}(1/|q|)$). The main feature of this model lies in the fact it can be solved exactly; the first bands $E_n(\kappa)\in[0,1]$ corresponding to bound eigenstates are solutions of the equation

$$\phi(E)=\frac{1-2E}{2\sqrt{E(1-E)}}\sinh(\beta\pi)\sin(\alpha\pi)+\cosh(\beta\pi)\cos(\alpha\pi)=\cos(2\pi\kappa) \tag{20}$$

with $\alpha=\sqrt{2E}$ and $\beta=\sqrt{2|1-E|}$. The next ones $E_n(\kappa)>1$ which correspond to the classical regime satisfy

$$\tilde{\phi}(E)=\frac{1-2E}{2\sqrt{E(E-1)}}\sin(\beta\pi)\sin(\alpha\pi)+\cos(\beta\pi)\cos(\alpha\pi)=\cos(2\pi\kappa). \tag{21}$$

For both examples, we display the numerical results $\kappa\mapsto E_n(\kappa)$ for $n=1,\ldots,5$ in Fig. 1 where we chose the size of the matrix H_κ to be 101×101. The band gaps are known to be of the order of $\hat{V}_q$ [2]. We also display in Figs. 2 and 3 the square of the modulations $|z_\kappa^n(y)|^2$ for the five first bands and $\kappa=0$. One can therefore observe the noticeable difference between the two bound states associated to the valence bands which are

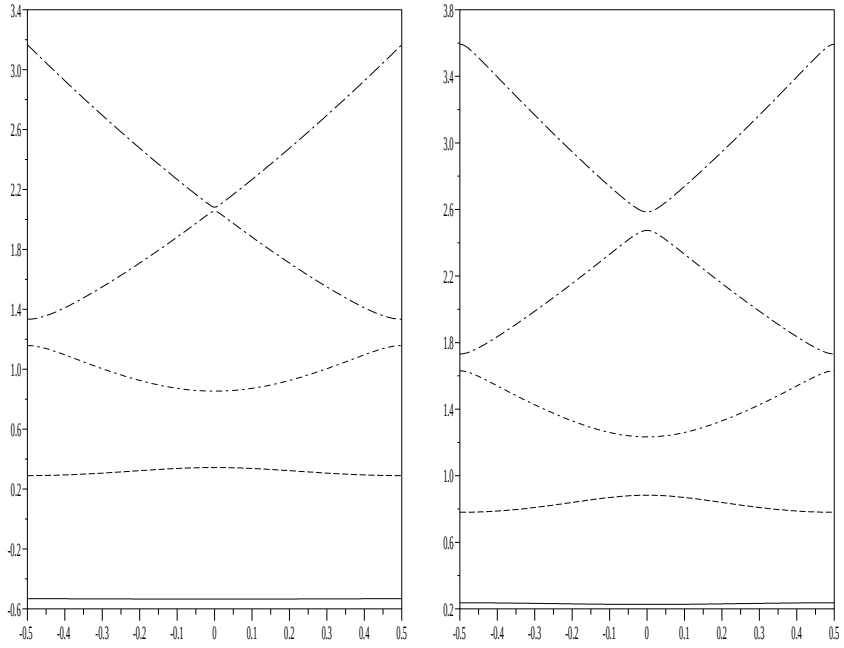

Fig. 1. Band structures for Mathieu's equation (left) and Kronig–Penney's model (right).

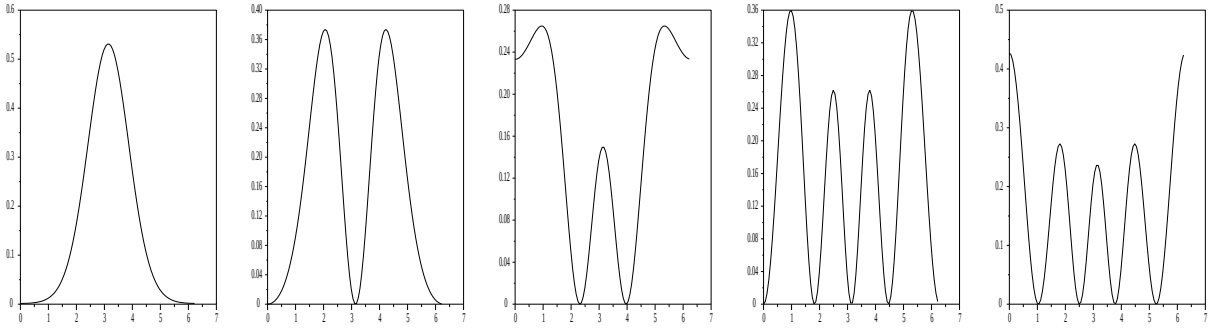

Fig. 2. Modulations $|(z^n_{\kappa=0}(x))|^2$ for Mathieu's potential; $n = 1, \ldots, 5$ (left to right).

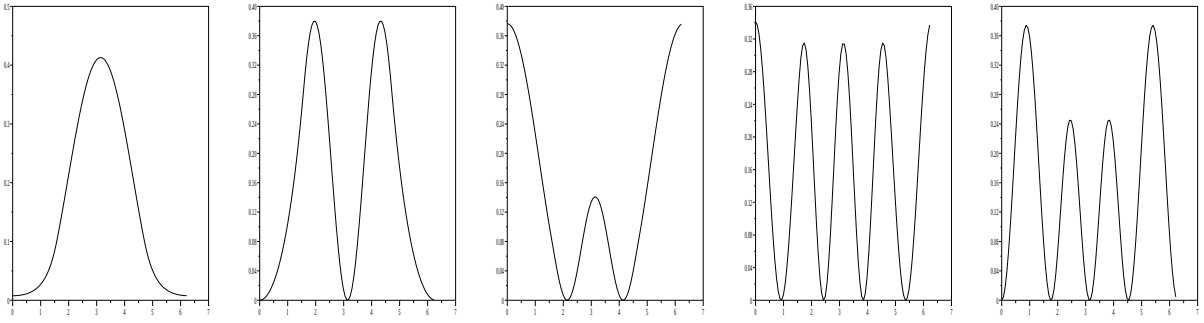

Fig. 3. Modulations $|(z^n_{\kappa=0}(x))|^2$ for Kronig–Penney's potential; $n = 1, \ldots, 5$ (left to right).

tightly sticked onto the atoms. In sharp contrast, the first conduction band shows very small position density in the vicinity of the atoms. As $E_n(\kappa)$ increases, one arrives in the classical regime and position densities of the corresponding Bloch states are less peaked.

2.3. Band transport equations

Typically, the Hamilton–Jacobi equation (12) (with $E = E_n$ for some value n of the band index) develops caustics in finite time, i.e. sets of singularities for the phase φ. Therefore, the WKB expansion is supposedly limited to local-in-time approximations of the wave function and its quadratic observables when classical singlevalued solutions of (12) are considered. Going beyond caustic onset is facilitated by "unfolding the caustics in phase space" [35]: this can be carried through relying on (band) Wigner transforms and their weak limits, the so-called (band) Wigner measures, as done in [27,42,46,49]. We now present a short summary of these results, focusing on what will be needed from a computational standpoint.

Let us first notice that the Bloch spectral problem (16) induces an orthogonal decomposition of the state space into wavepacket subspaces

$$L^2(\mathbb{R}) = \oplus_{n=1}^{\infty} \mathscr{S}_n^{\varepsilon}, \quad \mathscr{S}_n^{\varepsilon} = \left\{ \phi_n^{\varepsilon}(x) = \int_B \sigma(\kappa) \Psi_{\kappa}^n(x/\varepsilon) \, \frac{\mathrm{d}\kappa}{\sqrt{\varepsilon}}; \ \sigma \in L^2(B) \right\}.$$

Indeed one can write any function $\psi \in L^2(\mathbb{R})$ as

$$\psi(x) = \sum_{n=1}^{\infty} \psi_n^{\varepsilon}(x), \quad \psi_n^{\varepsilon} \in \mathscr{S}_n^{\varepsilon}, \tag{22}$$

together with

$$\psi_n^{\varepsilon}(x) = \int_{-1/2}^{1/2} \hat{\psi}^{\varepsilon}(\kappa, n) \Psi_{\kappa}^n(x/\varepsilon) \, \frac{\mathrm{d}\kappa}{\sqrt{\varepsilon}}, \quad \hat{\psi}^{\varepsilon}(\kappa, n) = \int_{\mathbb{R}} \psi(x) \bar{\Psi}_{\kappa}^n(x/\varepsilon) \, \frac{\mathrm{d}x}{\sqrt{\varepsilon}}. \tag{23}$$

The Schrödinger equation (6) with $V_e \equiv 0$ decouples into a series of "band equations":

$$\mathrm{i}\varepsilon \partial_t \psi_n^{\varepsilon} = E_n(\varepsilon D) \psi_n^{\varepsilon}, \quad n = 1, 2, \ldots, \tag{24}$$

where $E_n(\varepsilon D)$ is the pseudo-differential operator with Fourier multiplier $E_n(\varepsilon\kappa)$. The crucial feature that $E_n(\varepsilon D)$ leaves invariant the bandspace $\mathscr{S}_n^{\varepsilon}$ is generally lost when an exterior potential V_e is incorporated. The initial datum for (24) is obtained by L^2 projection of the initial wave function on each band space $\mathscr{S}_n^{\varepsilon}$ following (22) and (23). Then one sets up the band Wigner series $w_n^{\varepsilon}(t, x, \kappa)$ as in (3) for each ψ_n^{ε} and computes the corresponding time evolution equations from (24). It is meaningful to pass to the semiclassical limit $\varepsilon \to 0$ under the assumption that the nonnegative Borel measures

$$\forall n \in \mathbb{N}, \quad w_{n,I}(x, \kappa) = \lim_{\varepsilon \to 0} w_n^{\varepsilon}(t = 0, x, \kappa)$$

(where limits are possibly taken along subsequences) vanish on $\mathbb{R} \times C$, C standing for the set of band-crossing points. We thus obtain the transport equations for the limiting nonnegative bounded measures $w_n := \lim_{\varepsilon \to 0} w_n^{\varepsilon}$ as announced in (4), see [27,46] for more details

$$\forall n \in \mathbb{N}, \quad \partial_t w_n(t, x, \kappa) + E_n'(\kappa) \partial_x w_n(t, x, \kappa) = 0. \tag{25}$$

This Cauchy problem is solved easily for $t > 0$, $\kappa \in B$ and $x \in \mathbb{R}$,

$$w_n(t, x, \kappa) = w_{n,I}\big(x - t.E_n'(\kappa), \kappa\big)$$

and (for instance) the position density $\rho^\varepsilon(t,x)$ homogenizes in the following way:

$$\rho^\varepsilon(t,x) \overset{\varepsilon\to 0}{\rightharpoonup} \rho(t,x) = \int_B \sum_{n=1}^{\infty} w_{n,I}(x - t.E_n'(\kappa),\kappa)\,\mathrm{d}\kappa.$$

Assume now that the initial wave function is of the WKB type

$$\psi(t=0,x) = \sqrt{\rho_I(x)}\exp(\mathrm{i}\varphi_I(x)/\varepsilon),$$

where $\rho_I \in \mathbb{R}^+$ and $\varphi_I \in \mathbb{R}$ are smooth functions. It is an easy exercise to show that the weak limit of the band-Wigner function (3) associated to $\psi(t=0,.)$ as $\varepsilon \to 0$ is the monokinetic phase space measure

$$w(t=0,x,\kappa) = \rho_I(x)\delta_\#(\kappa - \partial_x\varphi_I(x)), \tag{26}$$

where $\delta_\#$ stands for the 2π-periodic Dirac distribution: $\delta_\# = \sum_{j\in\mathbb{Z}} \delta(. - 2j\pi)$.

Denote by $\mathscr{I}_n^\varepsilon$ the orthogonal $L^2(\mathbb{R})$-projector onto each one of the band-spaces $\mathscr{S}_n^\varepsilon$ defined at the beginning of this section

$$(\mathscr{I}_n^\varepsilon\psi)(t,x) = \psi_n^\varepsilon(t,x) = \int_{-\frac{1}{2}}^{\frac{1}{2}} \left(\int_{\mathbb{R}} \psi(t,y)\bar{\Psi}_\kappa^n(y/\varepsilon)\,\frac{\mathrm{d}y}{\sqrt{\varepsilon}}\right)\Psi_\kappa^n(x/\varepsilon)\,\frac{\mathrm{d}\kappa}{\sqrt{\varepsilon}},$$

and by $w_{n,I}^\varepsilon$ the band Wigner transform of $\mathscr{I}_n^\varepsilon\psi(t=0,.)$. If all the bands E_n are isolated (which is possible in one space dimension), there holds [27], Section 4:

$$w(t=0,x,\kappa) = \sum_{n\in\mathbb{N}} w_{n,I}(x,\kappa), \quad w_{n,I}^\varepsilon \overset{\varepsilon\to 0}{\rightharpoonup} w_{n,I}.$$

Since each $w_{n,I}$ is a bounded nonnegative measure, we conclude that it is supported inside the Lagrangian manifold $\{(x,\varphi_I(x)+2j\pi);\ x\in\mathbb{R}, j\in\mathbb{Z}\}$. Hence we have in the limit $\varepsilon\to 0$ "band monokinetic initial data":

$$\forall n\in\mathbb{N}, \quad w_{n,I}(x,\kappa) = \rho_{n,I}(x)\delta_\#(\kappa - \partial_x\varphi_I(x)). \tag{27}$$

In order to highlight consistency with the WKB ansatz (14), let us consider the WKB initial wave function

$$\tilde{\psi}_{n,I}^\varepsilon(x) = a_{n,I}(x)\exp(\mathrm{i}\varphi_I(x)/\varepsilon)z^n_{\partial_x\varphi_I}(x/\varepsilon). \tag{28}$$

At first sight, $\tilde{\psi}_{n,I}^\varepsilon \notin \mathscr{S}_n^\varepsilon$ for general φ_I and $a_{n,I}$ (i.e. $\varphi_I(x)\neq\kappa x$, $a_{n,I}(x)\neq 1/\sqrt{\varepsilon}$); but since

$$\forall n\in\mathbb{N}, \quad |z_\kappa^n(x/\varepsilon)|^2 \overset{\varepsilon\to 0}{\rightharpoonup} Z^n \in \mathbb{R}^+,$$

uniformly for $\kappa\in B$, a simple computation shows that the Wigner series $\tilde{w}_{n,I}^\varepsilon$ associated to (28) at $t=0$ satisfies

$$\tilde{w}_{n,I}^\varepsilon(x,\kappa) \overset{\varepsilon\to 0}{\rightharpoonup} |a_{n,I}(x)|^2 Z^n\delta_\#(\kappa - \partial_x\varphi_I(x)).$$

And what we obtain is nothing but monokinetic band Wigner measures of the type (27) at time $t=0$. Very recently, nonvanishing external potentials have been included in the analysis [12,34]; in this last case, the transport equation (25) is of Vlasov type and reads

$$\forall n\in\mathbb{N}, \quad \partial_t w_n + E_n'(\kappa)\partial_x w_n - V_e'(x)\partial_\kappa w_n = 0. \tag{29}$$

One recovers the Hamilton–Jacobi equation (12) from (25) by assuming furthermore that the nth band Wigner measure is monokinetic (27) [15,27]. Hence each of the nth band position densities satisfies a scalar conservation law whose velocity field is precisely $E_n'(\partial_x\varphi)$ if restricted to the time interval before caustic onset [15,49]. Also the limiting nth band density ρ_n is precisely the limit (as $\varepsilon \to 0$) of the sequence ρ_n^ε associated to (14) and (15)

$$\forall n \in \mathbb{N}, \quad \tilde{\rho}_n^\varepsilon := |\tilde{\psi}_n^\varepsilon|^2 \overset{\varepsilon\to 0}{\rightharpoonup} |a_n|^2 Z_n := \rho_n,$$

at least before caustic onset. In particular, the WKB reconstruction of the wave function (14) and (15) (together with its associated position density $\tilde{\rho}_n^\varepsilon$) is more precise than what comes out of the "totally homogenized" Cauchy problem for the band transport equation (25). We remark that the characteristic curves of the kinetic equations (25) and (26) are the Hamiltonian trajectories in phase space, ($\cdot$ standing for time-differentiation)

$$\dot{X} = E_n'(K), \quad \dot{K} = -V_e'(X), \tag{30}$$

along which the Borel measure w_n remains constant. Taking as an initial data

$$K(0) = \partial_x\varphi_I(X(0)), \quad X(0) = X \in \mathbb{R},$$

ones recovers precisely the rays of the Hamilton–Jacobi equation (12). Thus, from the standpoint of the semiclassical problem (6), this nonlinear equation becomes meaningless if globally understood in a monovalued (i.e. classical or viscosity) sense. Instead, a concept of multivalued solution relying on the validity of the bicharacteristics $t \mapsto (X,K)(t)$ associated to both Eq. (12) and the Hamiltonian system (30) beyond caustic onset must be considered. Hence the monokinetic density is replaced by a linear superposition

$$w(t,x,\kappa) = \sum_{k=1}^{N} \rho_k(t,x)\delta_\#(\kappa - \partial_x\varphi_k(t,x)), \quad \partial_x\varphi_k = u_k, \tag{31}$$

and the corresponding N-branch WKB ansatz of the wave function reads

$$\tilde{\psi}_n^\varepsilon(t,x) = \sum_{k=1}^{N} \sqrt{\mu_k(t,x)}\exp\left(\frac{\mathrm{i}}{\varepsilon}\varphi_k(t,x)\right) z_{u_k(t,x)}(x/\varepsilon). \tag{32}$$

However, solutions of the type (31) are more delicate to handle computationally [11,32,36,48] because it amounts to solving (or approximating by means of κ-moments) a transport equation in the sense of measures, see however [16,37]. Keeping in mind that our primary interest lies in the bicharacteristics of (30), (12) (or analogously the associated conservation law obtained by x-differentiation), we are about to show that they can be extracted from a simpler approach, namely the K-multivalued solutions in the sense of [14].

3. A general numerical strategy for multi-phase WKB

3.1. Introducing K-branch entropy solutions

In this subsection, we summarize the construction of nonnegative "multibranch solutions" of the Cauchy problem for 1D scalar balance laws with $uF'(u) \geqslant 0$

$$\partial_t u + \partial_x F(u) + G'(x) = 0, \tag{33}$$

under the nondegeneracy condition

$$\left|\left\{\xi \in \mathbb{R} \text{ such that } \tau + F'(\xi)\zeta = 0\right\}\right| = 0, \quad |\tau| = 1, \quad \zeta \in \mathbb{R},$$

through a kinetic formulation as in [14], see also [43,44,52]. Let $K \in \mathbb{N}$,

$$\Theta_K := \left\{\theta \in C^0(\mathbb{R});\ \partial_\xi^K \theta(\xi) \in \mathbb{R}_*^+ \text{ in } \mathscr{D}'(\mathbb{R})\right\},$$

are test-functions and, for some $L \in \mathbb{R}^+$,

$$\mathscr{F}_L := \left\{f \in L^\infty,\ 0 \leqslant f \leqslant 1 \text{ a.e. with } \mathrm{Supp}_\xi(f) \subset [0, L]\right\}$$

is a set of bounded kinetic densities with finite speed of propagation. Each $f \in \mathscr{F}_L$ induces a moment vector $\vec{m}(f) \in \mathbb{R}^K$ with components

$$m_k(f) = \int_{\mathbb{R}^+} \xi^{k-1} f(\xi)\, \mathrm{d}\xi, \quad k = 1, \ldots, K. \tag{34}$$

It is therefore possible to define the set of "realizable moments",

$$\mathbf{M}_K^L = \left\{\vec{m} \in \mathbb{R}^K; \exists f \in \mathscr{F}_L \text{ such that } \vec{m} = \vec{m}(f)\right\},$$

on which one formulates the following minimization problem:

$$\mathbf{J}_K^\theta(\vec{m}) = \inf_{f \in \mathscr{F}_L} \left\{ \int_{\mathbb{R}^+} \theta(\xi) f(\xi)\, \mathrm{d}\xi \text{ where } \vec{m}(f) = \vec{m} \in \mathbf{M}_K^L \text{ and } \theta \in \Theta_K \right\}.$$

It is shown in [14] that for any $\vec{m} \in \mathbf{M}_K^L$, there exists a unique solution of this problem called the *K-branch Maxwellian*. The minimizer is independent of the test-function $\theta \in \Theta_K$. It is determined by a vector of nonnegative real numbers $\vec{u} = (u_1, \ldots, u_K)$ in decreasing order and reads

$$\mathscr{M}_{K,\vec{m}}(u_1, \ldots, u_K, \xi) = \sum_{k=1}^{K} (-1)^{k-1} H(u_k - \xi), \quad u_k > u_{k+1} \geqslant 0, \tag{35}$$

where H stands for the Heaviside function. The "realizable moments" are given by the following map $\vec{m} : [0, L]^K \to \mathbf{M}_K^L$

$$m_\ell(u_1, \ldots, u_K) := \frac{1}{\ell} \sum_{k=1}^{K} (-1)^{k-1} (u_k)^\ell, \quad \ell = 1, \ldots, K. \tag{36}$$

It realizes a smooth one-to-one mapping of the u_k's as long as $u_k > u_{k+1}$ for all k under consideration. This leads to the following definition.

Definition 2 (*K-multivalued solutions* [14]). Any measurable function $\{0, 1\} \ni f(t, x, \xi)$ on $\mathbb{R}^+ \times \mathbb{R} \times \mathbb{R}^+$ satisfying the following kinetic equation in the sense of distributions

$$\partial_t f + F'(\xi)\partial_x f - G'(x)\partial_\xi f = (-1)^{K-1} \partial_\xi^K \tilde{m}, \quad f(t, x, \xi) = \mathscr{M}_{K,\vec{m}(f)} \tag{37}$$

with $\tilde{m}$ a nonnegative Radon measure on $\mathbb{R}^+ \times \mathbb{R} \times \mathbb{R}^+$ is a K-multivalued solution.

Theoretical results for K-multivalued solutions are provided in [14,52]. For $K > 1$, K-multivalued solutions generalize Kružkov's notion of bounded entropy solution of (33); in the special cases $K = 1$ and

$K = 2$, these statements coincide with the ones written in [43,44]. There is also equivalence between the kinetic equation and the hyperbolic system acting on the "realizable moments".

Theorem 2 (cf. [14]). *A measurable function $\mathscr{F}_L \ni f(t,x,\xi) = \sum_{k=1}^{K}(-1)^{k-1}H(u_k(t,x)-\xi)$ is a K-multivalued solution if and only if the entropy inequalities hold in $\mathscr{D}'(\mathbb{R}^+\times\mathbb{R})$ for any $\theta \in \Theta_K$:*

$$\partial_t \int_{\mathbb{R}^+} \theta(\xi) f(\xi)\,\mathrm{d}\xi + \partial_x \int_{\mathbb{R}^+} F'(\xi)\theta(\xi) f(\xi)\,\mathrm{d}\xi + G'(x)\int_{\mathbb{R}^+}\theta'(\xi) f(\xi)\,\mathrm{d}\xi \begin{cases} \leqslant 0, \\ = 0 \text{ if } \partial_\xi^K \theta \equiv 0. \end{cases} \tag{38}$$

For $\theta(\xi) = \xi^\ell$, $\ell = 0,1,\ldots,K-1$, one gets out of (38) the following set of K equations:

$$\partial_t \vec{m} + \partial_x \mathbf{F}_K(\vec{m}) + G'(x)\begin{pmatrix} 0 \\ m_1 \\ \vdots \\ (K-1)m_{K-1} \end{pmatrix} = 0, \quad m_{\ell+1}(t,x) = \int_{\mathbb{R}^+} \xi^\ell f(t,x,\xi)\,\mathrm{d}\xi. \tag{39}$$

This system is nonstrictly hyperbolic and diagonalizes in Riemann coordinates. For smooth solutions, the u_k's appearing in (35) are strong Riemann invariants and each one satisfies (33). System (39) is *strictly* hyperbolic if and only if they are all distinct; in this case, $u_k > u_{k+1}$ and the map $\vec{m}$ (36) is a diffeomorphism. It has been shown in [32] that this system is equivalent to the moment system obtained from (25) to (31) as long as K is big enough to keep $\tilde{m} \equiv 0$ in (37); more precisely, one has (see also Theorem 3.5 in [14]).

Theorem 3 (Equivalence of moment systems [32]). *Let $u_I := \partial_x \varphi_I$ be a smooth function and for some $n \in \mathbb{N}$, $\tilde{w}_n(t=0,x,\xi)$ be the solution of the Liouville equation (29) with initial condition, $\tilde{w}_n(t=0,x,\xi) = H(u_I - \xi)$. Consider the set*

$$\mathscr{C} = \left\{\xi \in \mathbb{R}^+ \text{ such that } \tilde{w}_n(t,x,\xi) = 1 \text{ for some } (t,x) \in \mathbb{R}^+\times\mathbb{R}\right\}.$$

Assume that $\mathscr{C}$ has only M connected components. If
(i) $M = (1/2)(K+1)$ (K *odd*) *or* $M = K/2$ (K *even*),
(ii) $N = K$ *in* (31),
then the moment systems obtained from (29) *with the Maxwellians* (31) *and* (35) *produce the same velocities* $u_k(t,x)$, $k = 1,2,\ldots,K$.

Theorem 3 ensures that the ansatz (35) can be used to obtain the velocities u_k's in the post-caustic onset representation of the solution (31) of the band transport equation (29) without having to handle weakly hyperbolic moment systems as in [36,48]. Then the corresponding densities ρ_k (or the intensities μ_k) are simply computed as a postprocessing relying on the exact solution of the linear continuity equation (13). Hence we introduce:

Definition 3 (*K-branch entropy solutions* [30]). A K-branch entropy solution of (33) is any set $\vec{u}$ of K nonnegative measurable functions $u_k(t,x)$ in $L^\infty(\mathbb{R}^+\times\mathbb{R})$ such that $u_k > u_{k+1}$ and for which (38) holds with $f(t,x,\xi) = \sum_{k=1}^{K}(-1)^{k-1}H(u_k(t,x)-\xi)$.

K-branch entropy solutions enjoy a "finite superposition principle" as shown in [48] since they match the solutions by characteristics [13,35] for K big enough. This last property is of special interest since the WKB system (15) has to be understood as a Correspondence Principle between quantum and classical mechanics. Since the Hamilton–Jacobi equation produces a possibly multivalued solution, we interpret it relying on the preceding framework; differentiating in the space variable, we pass from (12) to an equation of the type (33)

$$\partial_t u + \partial_x E_n(u) + V_e'(x) = 0, \quad F'(\xi) = E_n'(\xi), \quad G'(x) = V_e'(x). \tag{40}$$

K-branch entropy solutions produce an approximation of order ε to (6)–(10) for K big enough as they are concerned only with (12); to complete the ansatz, (13) has to be processed too. Indeed we shall see in the next section how to deduce very easily the corresponding intensities μ_k, $k = 1, 2, \ldots, K$ so as to keep the equivalence result of Theorem 3 with the N densities ρ_k in (31). Let us also mention that theoretical stability results are available in the strictly hyperbolic case and for $V_e' \in L^1 \cap L^\infty(\mathbb{R})$ as a byproduct of [1,9,28–30].

The choice of determining K with the purpose of representing all branches of the multivalued solution can be done in two ways: one relies on theoretical results concerning the singularities appearing in the solution and studied in e.g. [35,51] (see especially Theorem 4.1 in [51] where it is proven that the number of disjoint shock curves in Kružkov's solution of (33) is equal to the number of negative minima of $\partial_x F'(u_0)$ in case F is strictly convex) whereas the other is based on the remark that a shortage of moments manifests itself through the appearance of a compressive Lax's shock in the K-branch solution (see [32] for an illustration).

3.2. The general numerical procedure

All in all, a general computational approach for the homogenization-semiclassical limit of the Schrödinger equation (6) can be outlined:

- Determine the band structure and the Bloch states (cf. Section 2.2) and fix the band index $n \in \mathbb{N}$ corresponding to, say, the first conduction band.
- Determine the single-valued velocities $u_1, \ldots, u_K$ (making up altogether the multivalued velocity) as a K-branch entropy solution of (40) in the sense of Definition 3 with initial data (48).
- Compute each one of the corresponding intensities μ_k by solving (13) for the chosen band $\kappa \mapsto E_n(\kappa)$ of course using the same initial data.
- Set up the approximate K-branch wave function (32). Here the local phases φ_k are meant to satisfy $\partial_x \varphi_k = u_k$, $k = 1, \ldots, K$; the integration constants needed in order to fully determine them involve Maslov's phase-shifts, which are not however important in the context of approximation of quadratic observables. (A method for deriving directly multivalued phases without Maslov's indices has been recently presented in [16].)

  In particular, we shall approximate the position density in the following way:

$$\tilde{\rho}_n^\varepsilon(t,x) = \tilde{\psi}_n^\varepsilon \overline{\tilde{\psi}_n^\varepsilon}(t,x) = |\tilde{\psi}_n^\varepsilon(t,x)|^2 \simeq \sum_{k=1}^{K} \mu_k(t,x) |z_{u_k(t,x)}(x/\varepsilon)|^2, \tag{41}$$

together with the current density,

$$\tilde{J}_n^\varepsilon(t,x) = \varepsilon \Im\left(\overline{\tilde{\psi}_n^\varepsilon(t,x)} \partial_x \tilde{\psi}_n^\varepsilon(t,x)\right) \simeq \sum_{k=1}^{K} \mu_k(t,x) u_k(t,x) |z_{u_k(t,x)}(x/\varepsilon)|^2,$$

taking into account the fact that each of the cross-terms appearing when multiplying different branches of the WKB wave function should converge to zero weakly with $\varepsilon \to 0$, as shown by means of a (formal) computation based on the stationary phase lemma:

$$\forall t > 0, \quad \int_{\mathbb{R}} \sqrt{\mu_k \mu_{k'}(t,x)} \exp\left(\mathrm{i}(\varphi_k - \varphi_{k'})(t,x)/\varepsilon\right) z_{u_k}(x/\varepsilon) \overline{z_{u_{k'}}(x/\varepsilon)} \Phi(t,x)\, \mathrm{d}x$$

for all smooth test-function Φ can be written using Fourier series of the 2π-periodic modulations $z_\kappa(x)$ as follows:

$$\sum_{m,n\in\mathbb{Z}}\int_{\mathbb{R}}\sqrt{\mu_k\mu_{k'}(t,x)}\exp\left(\mathrm{i}(\varphi_k(t,x)-\varphi_{k'}(t,x)+(m-n)x)/\varepsilon\right)\hat{z}^m_{u_k}\overline{\hat{z}^n_{u_{k'}}}\Phi(t,x)\,\mathrm{d}x. \tag{42}$$

Thus the only contributions of order 1 as $\varepsilon\to 0$ stem from the stationary points of the function $S_{m,n}(x)=\varphi_k(t,x)-\varphi_{k'}(t,x)+(m-n)x$, i.e. $u_k(t,x)+m=u_{k'}(t,x)+n$ with $m,n\in\mathbb{Z}$. This means in particular that on caustic points where $u_k(t,x)=u_{k+1}(t,x)$ for some $k\in\mathbb{N}$, (41) would not be correct. In case $m\neq n$, taking velocities small enough (like $|u_k|<0.5$) can ensure that (41) will fail only in the neighborhood of caustics for small ε.

3.3. Fourier and parabolic band approximations

A genuine drawback is that the energy bands $\kappa\mapsto E_n(\kappa)$ are not known analytically; so the derivation of fluxes of the type $\int_{\mathbb{R}^+}E_n'(\xi)\theta(\xi)f(\xi)\,\mathrm{d}\xi$ inside the system (38) is not easy on a computational level. One way out will be to take advantage of the smoothness and symmetry of $E_n(\kappa)$ writing it as a Fourier series

$$E(\kappa)=\frac{\hat{E}_0}{2}+\sum_{q\in\mathbb{N}^*}\hat{E}_q\cos(2\pi q\kappa),\quad \hat{E}_q=4\int_0^{\frac{1}{2}}E(\kappa)\cos(2\pi q\kappa)\,\mathrm{d}\kappa. \tag{43}$$

We shall also use a more standard procedure as our main interest lies only in simulating the dynamics of the last valence and the first conduction bands (the second and third ones from bottom up in Fig. 1). Namely, the so-called parabolic band approximation consists in writing them as quadratic functions of the wavenumber, [2,47]

$$E_c(\kappa)\simeq E_c(0)+\frac{\kappa^2}{2m^*},\quad |\kappa|\ll\frac{1}{2}. \tag{44}$$

The number $m^*>0$ is called the electron's effective mass and heavily depends on the potential V through the bands diagram. In the case $V(x)=\cos(x)$, one finds the numerical values which give a good approximation for $|\kappa|\leqslant 0.3$,

$$m^*=0.2783,\quad E_c(0)=0.8536,$$

whereas the Kronig–Penney's model seems to be more restrictive with $|\kappa|\leqslant 0.2$ and

$$m^*=0.1915,\quad E_c(0)=1.2332.$$

Therefore, the WKB equations (15) boil down to

$$\partial_t\varphi+E_c(0)+\frac{1}{2m^*}(\partial_x\varphi)^2+V_e(x)=0;\quad \partial_t\mu+\frac{1}{m^*}\partial_x(\mu\partial_x\varphi)=0,\quad \mu=(a_n)^2. \tag{45}$$

Of course, this system bears a lot of similarities with the one studied in [30]. So, differentiating (45) with respect to x and interpreting the so-obtained scalar balance law relying on [14] yields for $f(t,x,\xi)=\sum_{k=1}^K(-1)^{k-1}H(u_k(t,x)-\xi)$

$$\partial_t\left(\int_{\mathbb{R}^+}\xi^\ell f(\xi)\,\mathrm{d}\xi\right)_{\ell=0,\dots,K-1}+\frac{1}{m^*}\partial_x\left(\int_{\mathbb{R}^+}\xi^{\ell+1}f(\xi)\,\mathrm{d}\xi\right)_{\ell=0,\dots,K-1}=\vec{0}, \tag{46}$$

which is a special case of (39). We shall limit ourselves mainly to the cases $K=2,3$. The intensities have to be sought as e.g. duality solutions [9] of the K continuity equations

$$\partial_t(\mu_\ell) + \frac{1}{m^*}\,\partial_x(u_\ell\ \mu_\ell) = 0, \quad \ell = 1,\dots,K. \tag{47}$$

The initial data for (46) are modified by a small parameter $|\eta| \ll 1$ in order to keep the system in a strictly hyperbolic region [30] and read

$$u_\ell(t=0,x) = \partial_x\varphi(t=0,x) - \eta\left(\ell - \frac{K+1}{2}\right), \quad \mu_\ell(t=0,x) = \mu(t=0,x). \tag{48}$$

4. Numerical processing of parabolic bands

4.1. Computation of the velocities and their corresponding intensities

From now on, we assume that the external potential V_e vanishes identically and we consider a uniform cartesian grid determined by the two positive parameters Δx, Δt which stand for the mesh-size and the time-step, respectively. We shall denote $x_j = j\Delta x$, $x_{j+1/2} = (j+1/2)\Delta x$, $t^n = n\Delta t$, and generic computational cells read

$$T_j^n = \left[t^n, t^{n+1}\right[\times \left[x_{j-\frac{1}{2}}, x_{j+\frac{1}{2}}\right[, \quad (j,n) \in \mathbb{Z}. \times \mathbb{N}.$$

As usual, the parameter λ will refer to $\Delta t/\Delta x$. Then, for a given $K > 1$, the grid functions $(\vec{m}_j^n, \vec{\mu}_j^n) \in (\mathbb{R}^K)^2$ stand for some numerical approximations of the moments in (46) $\vec{m}(t^n, x_j)$ and the intensities $\vec{\mu}(t^n, x_j)$ in (47) on each T_j^n. K-branch solutions are updated in time with an explicit Euler marching method

$$\vec{m}_j^{n+1} = \vec{m}_j^n - \frac{\lambda}{2m^*}\left(F_K(\vec{m}_j^n, \vec{m}_{j+1}^n) - F_K(\vec{m}_{j-1}^n, \vec{m}_j^n)\right), \quad j \in \mathbb{Z}.$$

Relying on previous experience [30–32], we selected the simple *local Lax–Friedrichs* (LLxF for short) numerical flux vector which in the present setting reads

$$F_K(\vec{m}_j^n, \vec{m}_{j+1}^n) = \left\{ \frac{1}{\ell}\sum_{k=1}^{K}(-1)^{k-1}\left[(u_k^\ell)_j^n + (u_k^\ell)_{j+1}^n\right] \right\}_{\ell=2,\dots,K+1} - \max_{k;j,j+1} |u_k|^n \left(\vec{m}_{j+1}^n - \vec{m}_j^n\right). \tag{49}$$

A crucial step lies clearly in finding out the relations between the moments m_k's and the Riemann coordinates u_k's; they constitute a Vandermonde system and have been solved in [48]. We recall briefly here the cases $K = 2$ and $K = 3$ since they correspond to the generic 1D singularities. From (36), we have

$$m_1 = u_1 - u_2, \quad m_2 = \frac{1}{2}\left((u_1)^2 - (u_2)^2\right),$$

and this can obviously be inverted

$$u_1 = \frac{m_2}{m_1} + \frac{m_1}{2}, \quad u_2 = \frac{m_2}{m_1} - \frac{m_1}{2},$$

in order to find the last component of the fluxes

$$m_3 = \frac{1}{3}\left((u_1)^3 - (u_2)^3\right) = \frac{(m_2)^2}{m_1} + \frac{(m_1)^3}{12}.$$

For $K = 3$, things get worse and following [48]

$$u_2 = \frac{-(m_1)^3 - 6m_3 + 6m_1m_2}{3\Big((m_1)^2 - 2m_2\Big)}, \quad u_{1,3} = \frac{4\Big((m_1)^3 - 3m_3\Big) \pm \sqrt{\Delta}}{12\Big((m_1)^2 - 2m_2\Big)},$$

where

$$\Delta = 16\Big((m_1)^3 - 3m_3\Big)^2 - 24\Big((m_1)^2 - 2m_2\Big)\Big((m_1)^4 + 12(m_2)^2 - 12m_3m_1\Big).$$

One can write $m_4 = (1/4)((u_1)^4 - (u_2)^4 + (u_3)^4)$ in terms of m_1, m_2, m_3 to close the system. At this point, one is able to propagate in time the $\vec{m}_j^n$ and thus the corresponding $\vec{u}_j^n$. We now explain how the intensities $\vec{\mu}_j^n$ can be deduced in order to keep the equivalence Theorem 3 true even for nontrivial initial densities ρ_I. The continuity equation of (45) implies for $k = 1, \ldots, K$,

$$\mu_k(t,x) = \mu_k(t=0,x_0)\left|\frac{\partial x_0}{\partial x}\right|,$$

$$x = x_0 + t.u_k(t=0,x_0)/m^* = x_0 + t.u_k(t,x)/m^*,$$

since the Hamilton–Jacobi equation is homogeneous and its characteristics are straight lines along which the u_k's are constant. Hence for any $x \in \mathbb{R}$ and $t > 0$, the starting point x_0 is explicitly known when having the values $u_k(t,x)$

$$x_0 = x - \frac{t.u_k(t,x)}{m^*} \Rightarrow \frac{\partial x_0}{\partial x} = 1 - \frac{t.\partial_x u_k(t,x)}{m^*}, \quad k = 1, \ldots, K.$$

Numerically, if $\vec{u}_j^n$ is known up to $n = t^n/\Delta t$ this last expression rewrites

$$\forall j \in \mathbb{Z}, \quad (\mu_k)_j^n = \mu\left(t=0, x_j - \frac{t^n(u_k)_j^n}{m^*}\right)\left|1 - \frac{t^n}{2m^*\Delta x}\Big((u_k)_{j+1}^n - (u_k)_{j-1}^n\Big)\right|.$$

The accuracy of the intensities $\vec{\mu}_j^n$ is considerably improved when compared to the results obtained with finite-differences in [30,31] and cheaper compared to [36,48]. The validity of this approach comes from the fact it is at least as accurate as the standard marching schemes studied in [31] and the discretizations used in [11,32]. Concerning the initial datum, we selected $\eta = \Delta x/100$.

4.2. The Mathieu equation: $V(x) = \cos(x)$

As an illustration of the preceding statements, we consider in this section a simulation of (45) and (46) for initial data modelling a self-interfering Gaussian pulse as in [30,32]

$$u_0(x) = 0.3\sin(x), \quad \mu_0(x) = \exp\Big(-(x-\pi)^2\Big).$$

In this case, we are in position to use the results of [51] to find out the correct value of K: the function $m^*\partial_x F'(u_0)(x) = u_0'(x) = 0.3\cos(x)$ has a unique negative minimum inside $[0, 2\pi]$, thus a unique shock curve is expected to appear in the Kružkov's entropy solution. This corresponds to a cusp according to [35] and therefore $K = 3$. The parameter 0.3 forces the K-branch solutions to remain inside the portion of the Brillouin zone where the parabolic approximation (44) holds true. Moreover, by (42), we can think that our approximations of the position density will be qualitatively correct since $|u_k(t,x)| \leqslant 0.3$ for $k = 1, 2, 3$ and

$t > 0$. We selected $\Delta x = 2\pi/512$, $\Delta t = \Delta x/1.3$ and iterated the scheme (49) up to $T = 3$ to obtain Fig. 5. These results suggest that the rendering of the trivalued solution is consistent with the ray-traced picture (30) away from phase transitions, i.e. points where the solution bifurcates from one to three values simultaneously. At these locations, undercompressive shocks moving at characteristic speed appear in $\vec{m}(t,.)$ [30,32]. The scheme (49) keeps away from these nonstrict hyperbolicity points and this has consequences on the intensities $\vec{\mu}(t,.)$. As already observed in [30,32], the N-wave developing around the sonic point $x = 0$ is not perfectly rendered and this becomes noticeable on $\vec{\mu}(t,.)$. In order to check consistency with the genuine Schrödinger equation, we simulated (2), (14) by means of a Fourier solver to compare the position densities for $\varepsilon = 1/5$, 1/10, 1/15,1/20, 1/30, 1/50; see Fig. 6.

We give here some details about the numerical solver we set up for solving (2), (14) in the special case $V(x) = \cos(x)$. Another possible strategy can be obtained from [5]. The ansatz (14) reads

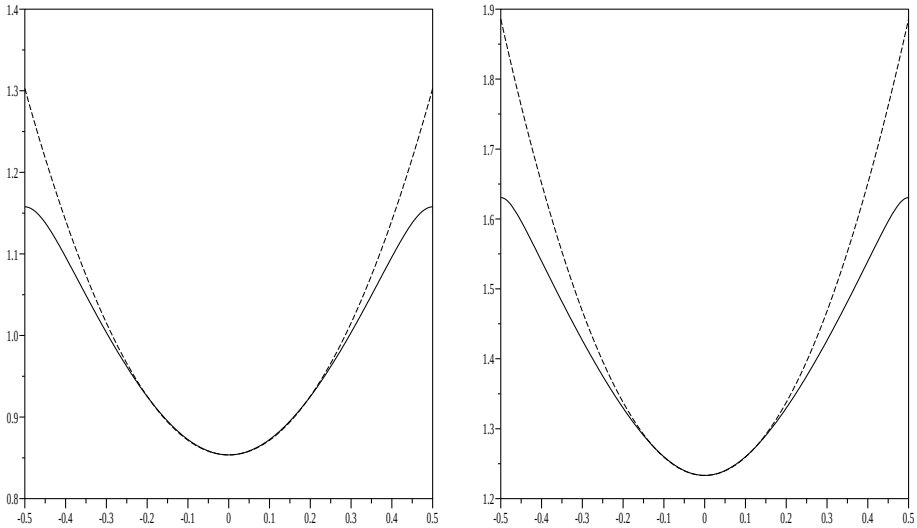

Fig. 4. Parabolic approximations (dotted lines) associated to the third bands in Fig. 1.

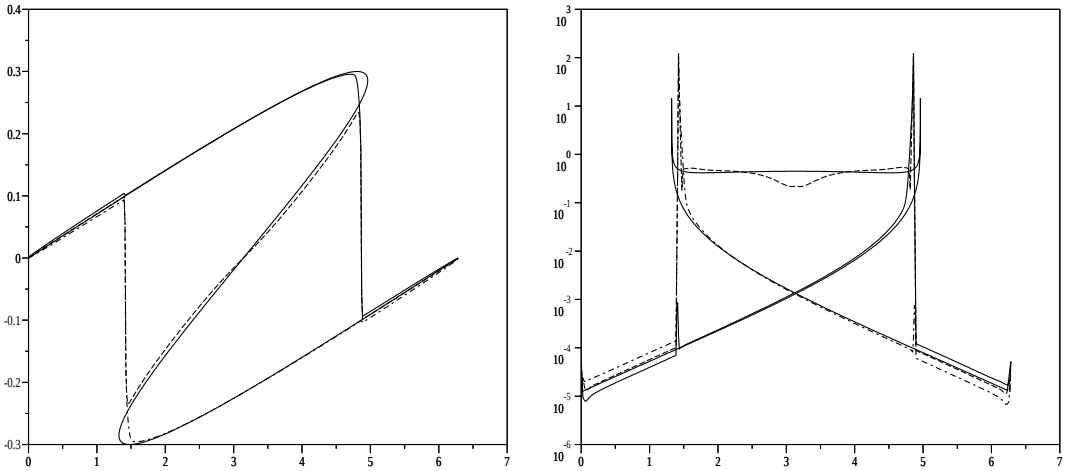

Fig. 5. Exact (solid lines) vs. numerical (dotted lines) velocities $\vec{u}(t = 3,.)$ (left) and intensities $\vec{\mu}(t = 3,.)$ (right).

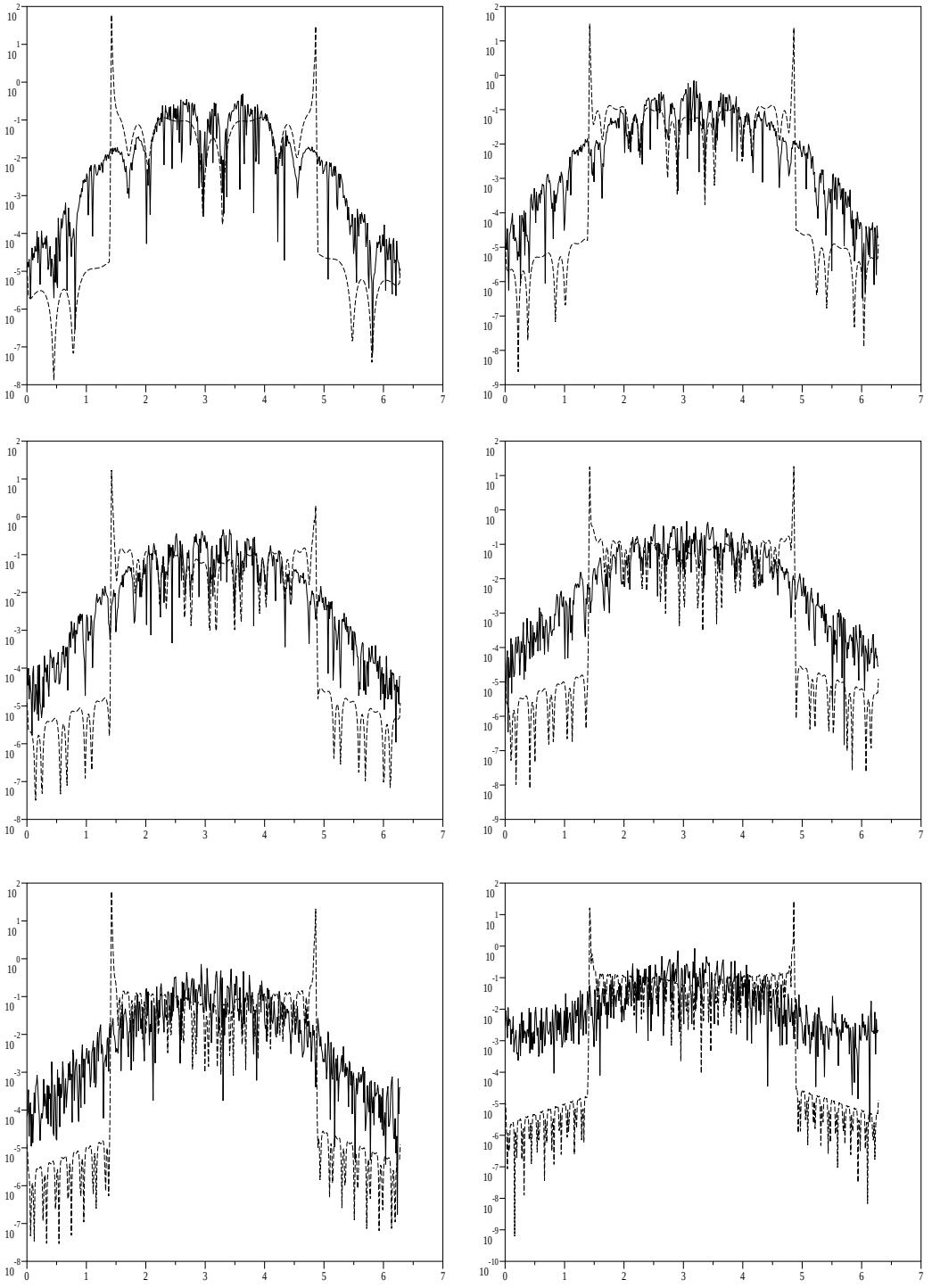

Fig. 6. Comparison between the WKB anzatz (14) (dotted lines) and the Fourier scheme (50) (solid lines) in $T = 3$.

$$\tilde{\psi}_n^{\varepsilon}(t=0,x)=\sqrt{\mu_0(x)}\exp(\mathrm{i}\varphi_0(x)/\varepsilon)z^n_{u_0(x)}(x/\varepsilon),\quad \partial_x\varphi_0(x)=u_0(x),$$

where $n=3$ corresponds to the first conduction band (see Figs. 1 and 2). We select an artificial period $L\in\mathbb{R}^+$ large enough to keep the aliasing effect small and expand $\psi(t,.)$ in its Fourier series for $x\in[0,L]$

$$\psi(t,x)=\sum_{q\in\mathbb{Z}}\hat{\psi}_q(t)\exp(2\pi\mathrm{i}qx/L),\quad \hat{\psi}_q(t)=\frac{1}{L}\int_0^L\psi(t,x)\exp(-2\pi\mathrm{i}qx/L)\,\mathrm{d}x.$$

We can now select values of ε such that $1/\varepsilon$ is an integer multiple of $2\pi/L$. Then, for all $t>0$, the Fourier coefficients $\hat{\psi}_q(t)$ satisfy the following differential system because for the Mathieu's equation, we have $V(x)=(\exp(\mathrm{i}x)+\exp(-\mathrm{i}x))/2$:

$$\forall q\in\mathbb{Z},\quad \mathrm{i}\varepsilon\frac{\mathrm{d}\hat{\psi}_q(t)}{\mathrm{d}t}=\frac{1}{2}\left(\hat{\psi}_{q-\frac{1}{2\pi\varepsilon}}(t)+q^2\varepsilon^2\hat{\psi}_q(t)+\hat{\psi}_{q+\frac{1}{2\pi\varepsilon}}(t)\right).\tag{50}$$

Of course, in practice, one has to consider a finite set of coefficients only, that is to say $\psi_q(t)\equiv 0$ for $|q|>M\in\mathbb{N}$: we chose $M=2048$ together with $L=2\pi$. The numerical comparison between the "3-branch position density" (41) and the one which is deduced from the Fourier scheme (50) suggest that the WKB approximation is qualitatively correct already for $\varepsilon=1/5$ away from the caustics (we stress that its accuracy is supposed to be of the order of $\varepsilon+\Delta x$). The low accuracy already noticed around the stagnation point $x=0$ can be observed again within this comparison for all values of ε. One can see that even if some noise affects the Schrödinger solution for some values of ε, the WKB structure and the modulations slowly emerge as $\varepsilon\to 0$. Despite the very large number of coefficients involved, the Fourier scheme seems to lose accuracy for $\varepsilon\leqslant 1/30$. In Fig. 7, a comparison is displayed for $\varepsilon=1/5,1/15,1/25,1/35$ in normal scale.

5. Computations inside the whole Brillouin zone

5.1. Velocities and intensities derivation

It is clear looking at Fig. 4 that the parabolic band approximation is only valid for a portion of the Brillouin zone B whose size depends on the bands structure induced by $V(x)$. It can cover 60% of B for the Mathieu's equation, but is shrinks to less than 40% for the Kronig–Penney's model. Hence in order to carry out high field simulations, one can feel the need for a more sophisticate approach still based on K-branch entropy solutions but taking into account for the whole band structure. Indeed, as the first conduction band $\kappa\mapsto E(\kappa)$ is 1-periodic, even and smooth even at the edges of the Brillouin zone, it can be written as a Fourier series (43) where the coefficients $\hat{E}_q$ decay very quickly with $q\in\mathbb{N}$. We display in Fig. 8 the resulting approximation for the conduction bands in Fig. 1. In order to cope with the framework presented in Section 2.3, we have now to consider that $F'(u)=E'(u)$ in (33) and this leads us to slightly more intricate moment systems

$$\partial_t\left(\int_{\mathbb{R}^+}\xi^\ell f(\xi)\,\mathrm{d}\xi\right)_{\ell=0,\dots,K-1}+\partial_x\left(\int_{\mathbb{R}^+}\xi^\ell E'(\xi)f(\xi)\,\mathrm{d}\xi\right)_{\ell=0,\dots,K-1}=\vec{0}.\tag{51}$$

Let us mention however that in this case, the resulting systems (51) are nonstrictly hyperbolic and nongenuinely nonlinear in the sense of Lax [3]. System (51) is hyperbolic since it has a convex entropy [14]. However, in the Riemann coordinates, it rewrites for smooth solutions

$$\partial_t u_k+E'(u_k)\partial_x u_k=0,\quad k=1,\dots,K.$$

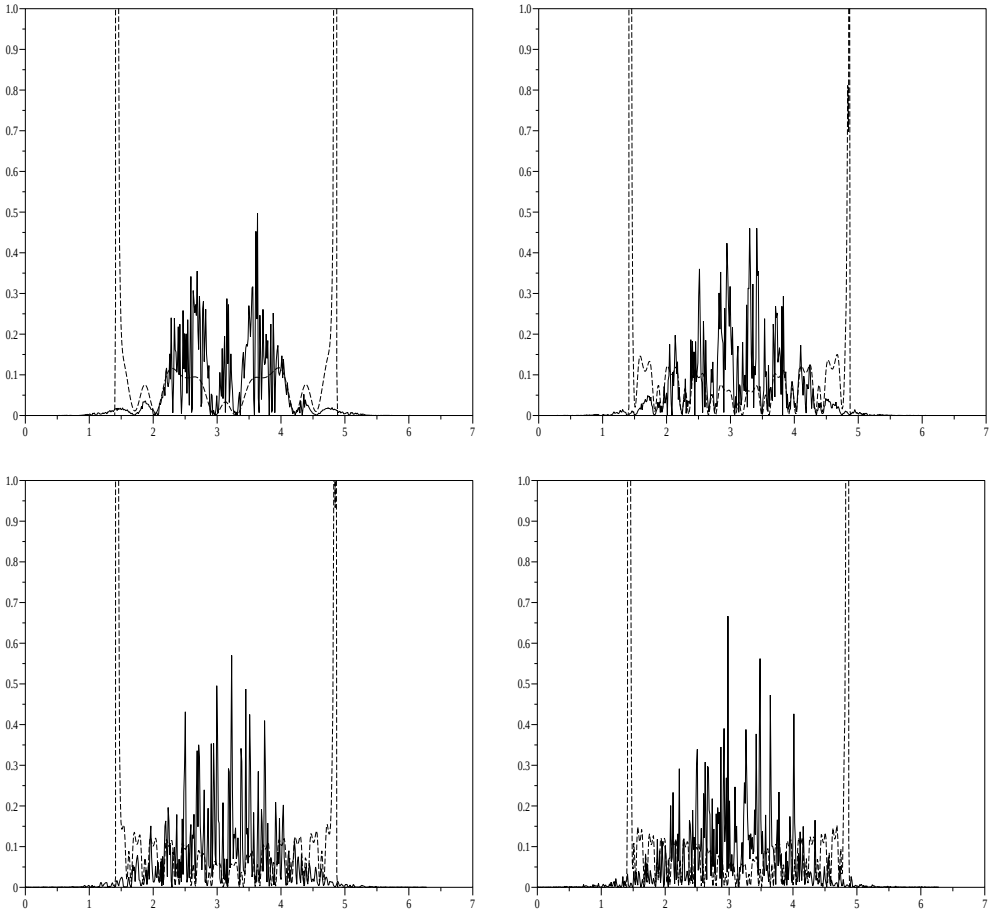

Fig. 7. Comparison between the (truncated) WKB anzatz (14) (dotted lines) and the Fourier scheme (50) (solid lines) in $T = 3$.

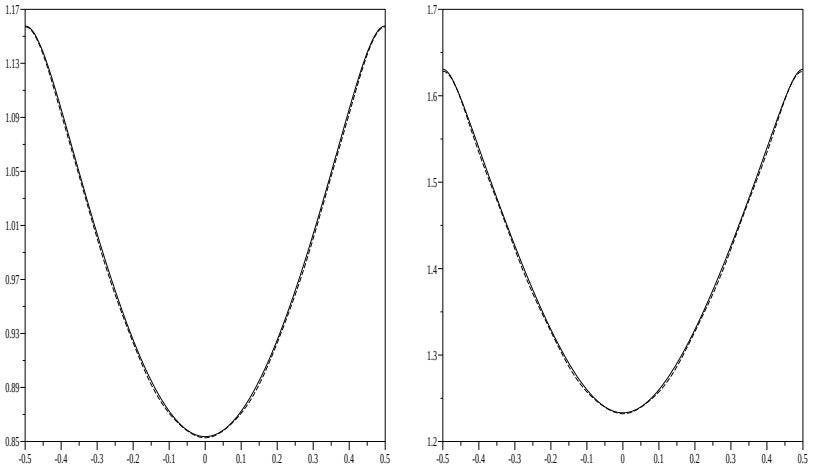

Fig. 8. Fourier approximations (dotted lines) associated to the third bands in Fig. 1.

Since $\kappa \mapsto E(\kappa)$ is 1-periodic, (51) is nongenuinely nonlinear and strict hyperbolicity is lost when $u_k = u_{k+1}$ for some k. We see that the fluxes appearing in (51) are given by integrals of the form

$$\int_{\mathbb{R}^+} \xi^\ell E'(\xi) f(t,x,\xi)\,\mathrm{d}\xi = \sum_{q\in\mathbb{N}^*} -\hat{E}_q \int_{\mathbb{R}^+} 2\pi q \xi^\ell \sin(2\pi q\xi) f(t,x,\xi)\,\mathrm{d}\xi,$$

where $\ell = 0,\ldots,K-1$ and $f(t,x,\xi) = \sum_{k=1}^{K}(-1)^{k-1}H(u_k(t,x)-\xi)$. It turns out that the right-hand side can be computed exactly with integrations by parts. For instance, in the cases $K = 2,3$, one has for any $\lambda \in \mathbb{R}$,

$$\int_0^u \xi\lambda \sin(\lambda\xi)\,\mathrm{d}\xi = -u\cos(\lambda u) + \frac{\sin(\lambda u)}{\lambda},$$

$$\int_0^u \xi^2\lambda \sin(\lambda\xi)\,\mathrm{d}\xi = -u^2\cos(\lambda u) + \frac{2u\sin(\lambda u)}{\lambda} + \frac{2(\cos(\lambda u)-1)}{\lambda^2}.$$

We follow the same lines as in the preceding section; of course the numerical fluxes are more involved and one must replace (49) with

$$F_K(\vec{m}_j^n, \vec{m}_{j+1}^n) = \left\{ \sum_{k=1}^{K}(-1)^{k-1} \left(\int_0^{(u_k^\ell)_j^n} + \int_0^{(u_k^\ell)_{j+1}^n} \right) \xi^{\ell-1} E'(\xi)\,\mathrm{d}\xi \right\}_{\ell=1,\ldots,K} - \max_{k;\,j,j+1} |E'(u_k)|^n \left(\vec{m}_{j+1}^n - \vec{m}_j^n\right). \tag{52}$$

In order to complete the ansatz (14), we still have to deduce the values of $\vec{\mu}(t^n, x_j)$ for j,n in $\mathbb{Z}\times\mathbb{N}$. This will be done accordingly; for all k under consideration, we deduce from (13) that

$$\mu_k(t,x) = \mu_k(t=0,x_0)\left|\frac{\partial x_0}{\partial x}\right|, \quad x = x_0 + t.E'(u_k(t,x)),$$

and this paves the way for recovering numerically the $\vec{\mu}_j^n$ out of the set of $\vec{u}_j^n$ for all $j\in\mathbb{Z}$, $k = 1,\ldots,K$, with the formula

$$(\mu_k)_j^n = \mu\left(t=0, x_j - t^n E'\left((u_k)_j^n\right)\right)\left|1 - \frac{t^n}{2\Delta x}\left(E'((u_k)_{j+1}^n) - E'((u_k)_{j-1}^n)\right)\right|.$$

We chosed to limit ourselves to eight Fourier coefficients in (43) for the computations.

5.2. The Mathieu equation revisited

We first simulated the 3-branch entropy solutions by means of (51) and (52). Furthermore, the corresponding intensities have been derived accordingly. The parameters used were $\Delta x = \Delta t = 2\pi/512$ The consistency with the ray-traced solution (30) is clear in Fig. 9 despite the fact that u_0 covers a large part of the Brillouin zone. In particular, the parabolic band approach of Section 4.2 would produce a very poor approximation because $E'(\min(u_0)) = E'(\max(u_0)) = 0$. We consider $V(x) = \cos(x)$ inside (2) with the ansatz (14) where

$$u_0(x) = \frac{1}{2}\exp\left(-(x-\pi)^2\right), \quad \mu_0(x) = \frac{1}{\pi}\exp\left(-(x-\pi)^2\right),$$

which implies that

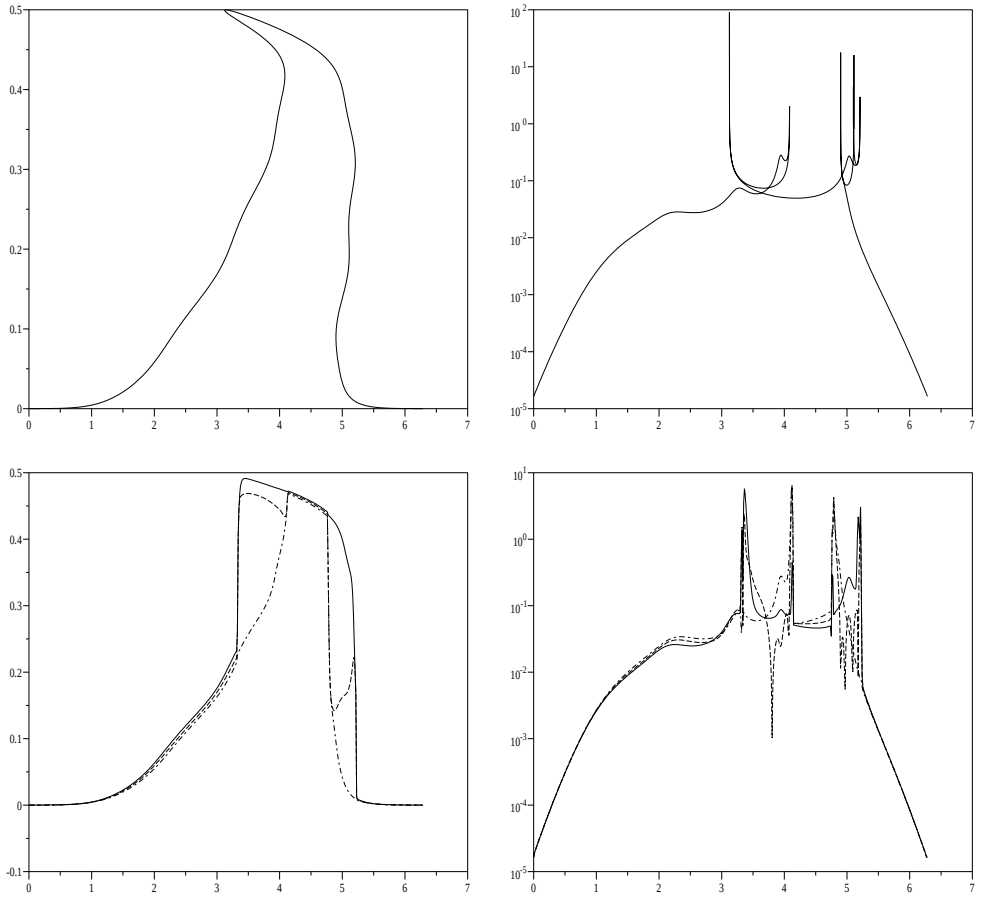

Fig. 9. Exact (top) vs. numerical (bottom) velocities $\vec{u}(1.5,.)$ and intensities $\vec{\mu}(1.5,.)$.

$$\varphi_0(x) = \frac{\sqrt{\pi}}{4}(\mathrm{erf}(\pi) + \mathrm{erf}(x-\pi)), \quad \mathrm{erf}(x) = \frac{2}{\sqrt{\pi}}\int_0^x \exp(-s^2)\,\mathrm{d}s.$$

In Fig. 9, one can observe two distinct multivalued zones which appear to be rendered differently. The first one ($x \in [3, 4.2]$) is fully developed and quite well approximated by the K-branch solution; however, the second one ($x \in [4.7, 5.3]$) is much narrower and the N-wave is not very good. This will have consequences when deducing quadratic observables like the position density. Hence we also wanted to check again the consistency with a direct simulation of (2) by means of (50) with $M = 2048$. In Fig. 10, we display the outcome of both approaches for $\Delta t = \Delta x = 2\pi/512$ in $T = 1.5$ for $\varepsilon = 1/5, 1/10, 1/15, 1/20, 1/30, 1/50$; at this time, the multivalued solution developed several caustics inside the interval $x \in [3, 6]$; we observe that in the region $x \in [3.5, 4.5]$, the WKB approximation behaves quite well. We also see perfect agreement for $\varepsilon \in [1/20, 1/5]$ inside the domain $x \in [0, 1] \cup [5, 2\pi]$; for $\varepsilon \leqslant 1/30$, the Fourier scheme seems to be overwhelmed. Before this happens, we observe some sort of slow and oscillatory decay, especially inside the Whitham's region $x \in [3, 6]$; in particular, signals propagate at a correct speed. The gap between the two numerical solutions remains at a correct level except at the blow-up points: this last feature being an inherent defect of the semiclassical WKB approach; cf. [45]. Moreover inside certain portions of the computational domain, the agreement between the two numerical strategies seems to hold pointwise. In any

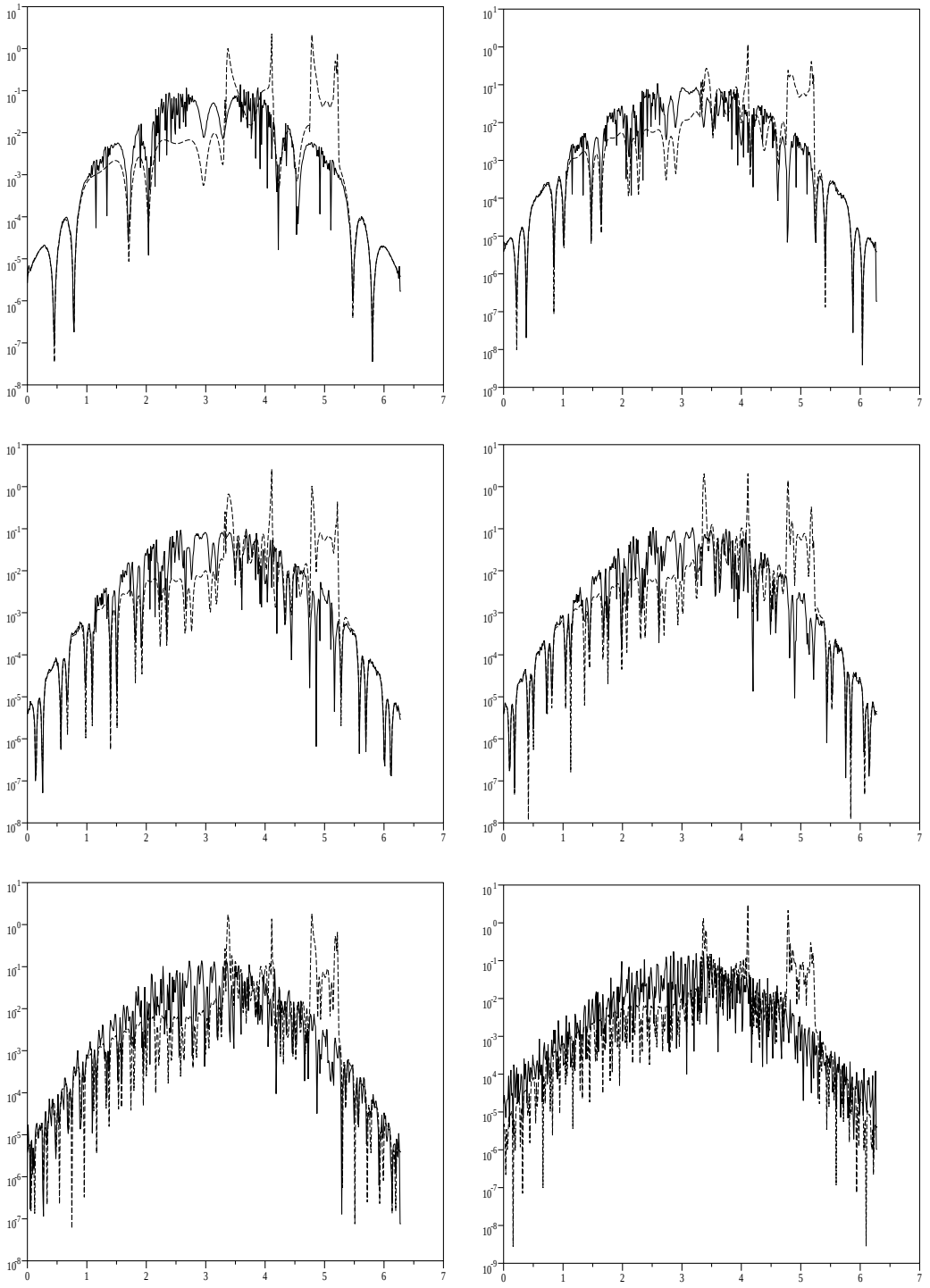

Fig. 10. Comparison between the WKB anzatz (14) (dotted lines) and the Fourier scheme (50) (solid line) in $T = 1.5$.

case, it looks much better than the parabolic band approximation, Figs. 6 and 7. A comparison in normal scale is displayed in Fig. 11 for $\varepsilon = 1/5, 1/15, 1/25, 1/35$.

5.3. The discontinuous Kronig–Penney model

We now switch to the potential (19) together with similar initial data

$$u_0(x) = \frac{1}{2}\exp\Big(-(x-\pi)^2\Big), \quad \mu_0(x) = \frac{1}{\pi}\exp\Big(-2(x-\pi)^2\Big).$$

Once again, a good agreement is observed between the ray-traced solution (30) and the 3-branch solutions we got out of (51), (52) after breakup at time $T = 1.05$; see Fig. 12. Two differences appear when comparing with Mathieu's equation: stronger oscillations show up on the intensities $\vec{\mu}$ and the (supposedly steady) nonstrict hyperbolicity point $\max(\vec{u})$ is not well rendered. This is related to the fact that $B \ni \kappa \mapsto E(\kappa)$ varies much more (as can be checked in Fig. 8). Thus the effect of numerical viscosity is noticeable; the parameters used were $\Delta x = 2\pi/512$ and $\Delta t = 0.8\Delta x$. We close this section mentioning that

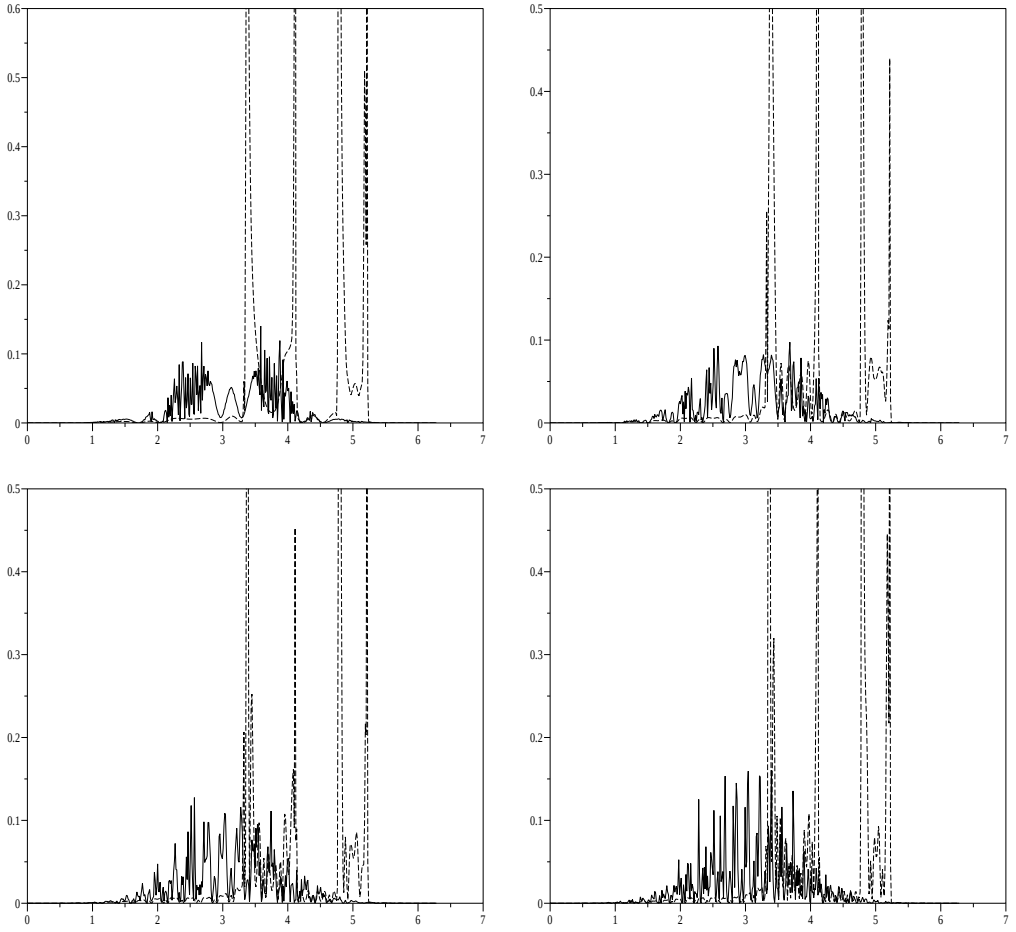

Fig. 11. Comparison between the (truncated) WKB anzatz (14) (dotted lines) and the Fourier scheme (50) (solid lines) in $T = 1.5$.

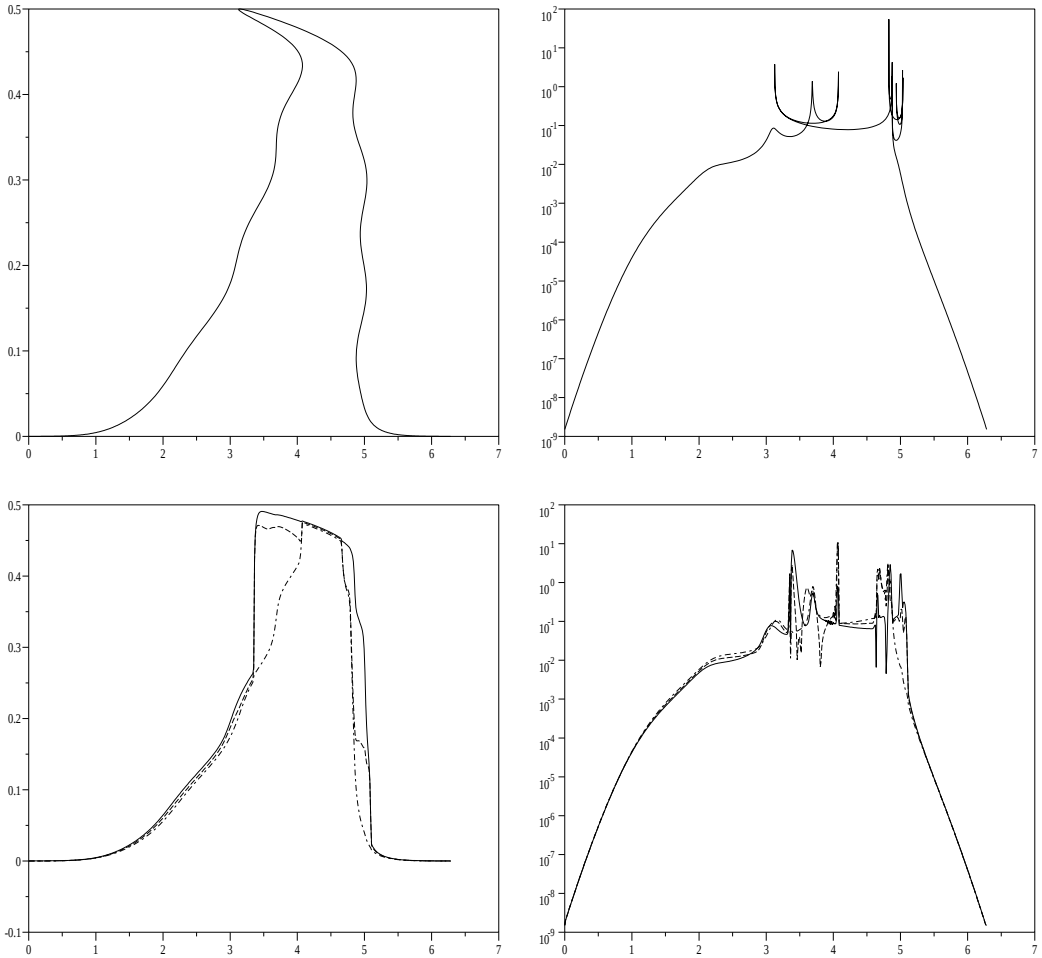

Fig. 12. Exact (top) vs. numerical (bottom) velocities $\vec{u}(1.05,.)$ and intensities $\vec{\mu}(1.05,.)$.

the Fourier scheme (50) extends easily to this case relying on the Fourier decomposition of the considered potential $V(x)$ (which is known to be 2π-periodic):

$$V(x) = \sum_{\ell\in\mathbb{Z}} \hat{V}_\ell \exp(\mathrm{i}\ell x), \quad \hat{V}_\ell = \frac{1}{2\pi}\int_0^{2\pi} V(x)\exp(-\mathrm{i}\ell x)\,\mathrm{d}x.$$

Hence, for $L = 2\pi$, the differential system (50) is modified accordingly for $1/\varepsilon \in \mathbb{N}$:

$$\forall q \in \mathbb{Z}, \quad \mathrm{i}\varepsilon\frac{\mathrm{d}\hat{\psi}_q(t)}{\mathrm{d}t} = \frac{q^2\varepsilon^2}{2}\hat{\psi}_q(t) + \sum_{\ell\in\mathbb{Z}} V_\ell\hat{\psi}_{q-\ell/\varepsilon}.$$

Of course, as in Section 3.2, one can only consider a finite number of Fourier coefficients when integrating this differential system. Actually this enlightens the big difficulty lying in a direct numerical simulation of the semiclassical limit $\varepsilon \to 0$: namely, with smaller ε, the periodic potential affects higher and higher fre-

quencies. The situation gets even worse when low-regularity potentials are involved for which the coefficients $\hat{V}_\ell$ do not decay quickly with $|\ell| \to +\infty$.

6. Conclusion and perspectives

So far, we have dealt with basic cases where short-scale periodic potentials take into account only for interaction with atoms of identical nature inside the crystal. Now, suppose that we add an impurity from column V in the Periodic Table to a semiconductor such as Silicon or Germanium which are both in column IV. This impurity atom will have one more electron that is needed to satisfy the valency requirements for the tetrahedral bonds formed with four electrons. This extra electron will be free to wander through the crystal lattice subject of course to Coulomb attraction of the ion core which will have one unit of positive charge. We are led to consider a slightly more complex Schrödinger equation in place of (1),

$$\mathrm{i}\hbar\partial_t\psi + \frac{\hbar^2}{2m}\partial_{xx}\psi = e\left(V(x) - \frac{e}{\epsilon_0|x - x_{\mathrm{donor}}|}\right)\psi, \tag{53}$$

and $\epsilon_0 \in [1, 100]$ (see [2, p. 578]) stands for an average dielectric constant seen by the donor's electron inside the crystal [2]. Reformulating (53) in atomic units $e = m = \hbar = 1$ ans assuming that V is 2π-periodic on the atomic length scale, the macroscopic scaling is determined by the slowly varying perturbation

$$\varepsilon = \frac{1}{\epsilon_0}, \quad \mathrm{i}\varepsilon\partial_t\psi + \frac{\varepsilon^2}{2}\partial_{xx}\psi = \left(V\left(\frac{x}{\varepsilon}\right) - \frac{1}{|x - \varepsilon x_{\mathrm{donor}}|}\right)\psi \tag{54}$$

and one deduces from band Wigner theory, see Section 2.3 and [2,12,27,34,47], that the dynamics of (54) are given by the nth band Hamiltonian: $E_n(p) - 1/|x - \varepsilon x_{\mathrm{donor}}|$. This way, the WKB systems (15) are now endowed with a source term

$$\partial_t\varphi + E_n(\partial_x\varphi) = \frac{1}{|x - \varepsilon x_{\mathrm{donor}}|}, \quad \partial_t\mu + \partial_x\big(\mu\, E_n'(\partial_x\varphi)\big) = 0. \tag{55}$$

Taking x-derivatives, one finds out that $F = E_n$ and $G(x) = -1/|x - \varepsilon x_{\mathrm{donor}}|$ in (33). Thus K-branch solutions are to be processed using sophisticate well-balanced techniques as in [1,30,32], but in a nonconvex and nonstrictly hyperbolic context. These topics will be developed in the forthcoming Part II of this work.

Appendix A. Naive WKB and effective Hamiltonians

We saw at the beginning of Section 2 that in the simplest case $V_e \equiv 0$, a naive WKB approach (8) leaves us with

$$\partial_t\varphi^\varepsilon + \frac{1}{2}(\partial_x\varphi^\varepsilon)^2 + V\left(\frac{x}{\varepsilon}\right) = 0$$

and this Eikonal equation can possibly be homogenized following [19,20,41] in order to get rid of the fast scale $y = x/\varepsilon$. By construction $x \mapsto \mathscr{H}(p, x)$ is 2π-periodic and we can seek the limiting behaviour of viscosity solutions φ^ε. Indeed, under mild hypotheses, $\varphi^\varepsilon \to \varphi$ satisfying in the sense of viscosity

$$\partial_t\varphi + \bar{\mathscr{H}}(\partial_x\varphi) = 0, \tag{A.1}$$

where $p \mapsto \bar{\mathscr{H}}(p)$ is the effective Hamiltonian whose derivation goes as follows. One considers the so-called "cell problem",

$$\mathscr{H}(p+\partial_y v(y),y)=\alpha,\quad (y,p)\in\mathbb{R}^2. \tag{A.2}$$

Then it is proved in [19,41] that for a given $p\in\mathbb{R}$, there is a unique $\alpha=\alpha(p)\in\mathbb{R}$ such that (A.2) admits a (possibly not unique) 2π-periodic viscosity solution $y\mapsto v(y)$. Hence the effective Hamiltonian in (A.1) reads

$$\bar{\mathscr{H}}(p)=\alpha.$$

This has connections with both classical (a so-called "generating function of a canonical transformation" u [25,38] is $u(y)=py+v(y)$ when v is smooth) and quantum mechanics. In fact, following [24], we consider the eigenproblem (11) and assume for Ψ:

$$\Psi(y)=\exp(\mathrm{i}py)\phi(y),\quad \phi(y)=a(y)\exp(\mathrm{i}v(y)).$$

Then, from (11), we deduce

$$\frac{1}{2}|p+\partial_y v(y)|^2+V(y)=E(p)+\frac{\partial_{yy}a}{2a},\quad \partial_y\Big(a(y)^2(p+\partial_y v)\Big)=0.$$

This hints that $\bar{\mathscr{H}}(p)=E(p)$ is related to the Bloch spectrum of $\mathscr{H}(y,\hat{p})$ for those bands for which the amplitude variations are small. We can go a bit further for instance considering the particular case $V(y)=\cos(y)$ inside (A.2)

$$v(y)=-py\pm\int_0^y\sqrt{2(\bar{\mathscr{H}}(p)-\cos(s))}\,\mathrm{d}s,\quad y\in[0,2\pi].$$

Two cases occur:

- if $\bar{\mathscr{H}}(p)\geqslant\max(\cos(y))$, then $v\in C^1_{\mathrm{per}}(\mathbb{R})$. A consequence of 2π-periodicity is

$$v(0)=0=v(2\pi)\Rightarrow p=\pm\frac{1}{2\pi}\int_0^{2\pi}\sqrt{2(\bar{\mathscr{H}}(p)-\cos(s))}\,\mathrm{d}s.$$

And this equation has a solution for

$$|p|\geqslant\frac{1}{2\pi}\int_0^{2\pi}\sqrt{2(1-\cos(s))}\,\mathrm{d}s=\frac{4}{\pi}.$$

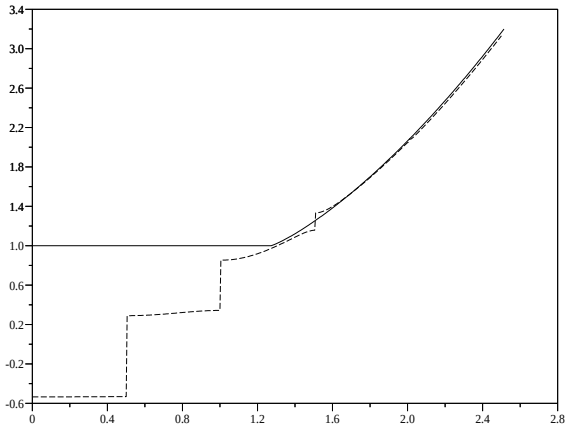

Fig. 13. Comparison between $\bar{\mathscr{H}}(p)$ (solid line) and the band structure (dotted line) for $V(x)=\cos(x)$.

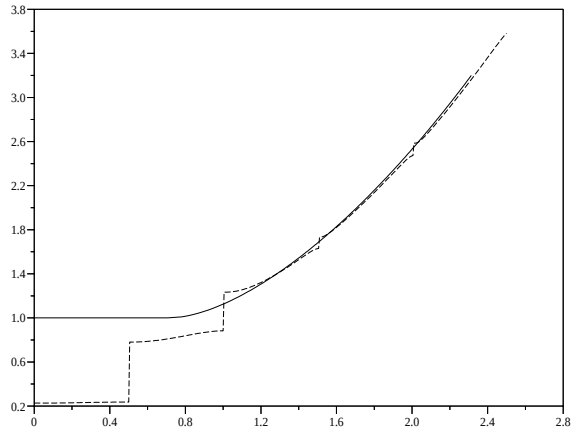

Fig. 14. Comparison between $\bar{\mathscr{H}}(p)$ (solid line) and the band structure (dotted line) for Kronig–Penney's model.

- if $\bar{\mathscr{H}}(p) < \max(\cos(y))$, then following [41], we take $\bar{\mathscr{H}}(p) \equiv 1 = \max(\cos(x))$.
  All in all, this technique gives:

$$\begin{cases} |p| = \frac{1}{2\pi}\int_0^{2\pi} \sqrt{2(\bar{\mathscr{H}}(p) - \cos(s))}\,\mathrm{d}s & \text{for } |p| \geqslant \frac{4}{\pi}, \\ \bar{\mathscr{H}}(p) \equiv 1 = \max(\cos(y)) & \text{for } |p| < \frac{4}{\pi}. \end{cases}$$

One recognizes some kind of Bohr–Sommerfeld quantization rule which gives flat bands in the nonclassical regime $E(p) < \max(V(y))$; see [18,38]. We are displaying $E_1(\kappa)$, $E_2((\kappa - \frac{1}{2}) + 1)$, $E_3(\kappa + 1)$, $E_4((\kappa - \frac{1}{2}) + 2)$, $E_5(\kappa + 2)$ for $\kappa \in [0, \frac{1}{2}]$ in order to compare with $p \mapsto \bar{\mathscr{H}}(p)$. This is inspired by the "nearly free electron model" [2]. When comparing with Fig. 4, one notices that for $|\kappa| = \frac{4}{\pi} - 1 \simeq 0.2732$, the first conduction band enters into the classical regime, i.e. $E_3(\kappa) > 1$. An illustration is provided within Fig. 13.

So, this process is not well-suited for our program because it would imply for instance an infinite effective mass for the electron since the parabolic band approximation (44) would essentially be

$$E_3(p) = E_3(0) = 1.$$

In the case of the discontinuous Kronig–Penney's model, one obtains a very simple simple formula for $\bar{\mathscr{H}}$

$$\begin{cases} |p| = \frac{1}{2}\left(\sqrt{2\bar{\mathscr{H}}(p)} + \sqrt{2(\bar{\mathscr{H}}(p) - 1)}\right) & \text{for } \bar{\mathscr{H}}(p) \geqslant 1, \\ \bar{\mathscr{H}}(p) \equiv 1 = \max(V(y)) & \text{otherwise.} \end{cases}$$

See the numerical results in Fig. 14.

References

[1] D. Amadori, L. Gosse, G. Guerra, Global BV entropy solutions and uniqueness for hyperbolic systems of balance laws, Arch. Rational Mech. Anal. 162 (2002) 327–366.
[2] N.W. Ashcroft, N.D. Mermin, Solid-state Physics, Rinehart and Winston, Holt, 1976.
[3] F. Ancona, A. Marson, A wave front tracking algorithm for $N \times N$ non genuinely nonlinear conservation laws, J. Differential Equations 177 (2001) 454–493.

[4] G. Bal, A. Fannjiang, G. Papanicolaou, L. Ryzhik, Radiative transfer in periodic structure, J. Stat. Phys. 95 (1999) 479–494.
[5] W.Z. Bao, S. Jin, P.A. Markowich, On time-splitting spectral approximations for the Schrödinger equation in the semiclassical regime, J. Comput. Phys. 175 (2002) 487–524.
[6] J.D. Benamou, Direct computation of multivalued phase space solutions for Hamilton–Jacobi equations, Commun. Pure Appl. Math. 52 (1999) 1443–1475.
[7] A. Bensoussan, J.L. Lions, G. Papanicolaou, Asymptotic Analysis for Periodic Structures, North-Holland, Amsterdam, 1978.
[8] F. Bloch, Über die quantenmechanik der electronen in kristallgittern, Z. Phys. 52 (1928) 555–600.
[9] F. Bouchut, F. James, One-dimensional transport equations with discontinuous coefficients, Nonlinear Anal. TMA 32 (1998) 891–933.
[10] F. Bouchut, F. James, Duality solutions for pressureless gases, monotone conservation laws and uniqueness, Commun. PDE 24 (1999) 2173–2189.
[11] F. Bouchut, S. Jin, X. Li, Numerical approximations of pressureless and isothermal gas dynamics, SIAM J. Numer. Anal. 41 (2003) 135–158.
[12] M. Brassart, Limite semi-classique de transformée de Wigner dans des milieux périodiques ou aléatoires, Ph.D. Thesis, Univ. de Nice, France, 2002.
[13] Y. Brenier, Averaged multivalued solutions for scalar conservation laws, SIAM J. Numer. Anal. 21 (1984) 1013–1037.
[14] Y. Brenier, L. Corrias, A kinetic formulation for multibranch entropy solutions of scalar conservation laws, Ann. IHP Nonlinear Anal. 15 (1998) 169–190.
[15] Y. Brenier, E. Grenier, Sticky particles and scalar conservation laws, SIAM J. Numer. Anal. 35 (1998) 2317–2328.
[16] L.-T. Cheng, H. Liu, S.J. Osher, High-frequency wave propagation in Schrödinger equations using the level set method, Commun. Math. Sci. 1 (3) (2003) 593–621.
[17] M. Christ, A. Kiselev, WKB and spectral analysis of one-dimensional Schrödinger operators for slowly varying potentials, Commun. Math. Phys. 218 (2001) 245–262.
[18] Y. Colin de Verdière, B. Parisse, Singular Bohr–Sommerfeld rules, Commun. Math. Phys. 205 (1999) 459–500.
[19] M.C. Concordel, Periodic homogenization of Hamilton–Jacobi equations: additive eigenvalues and variational formula, Indiana Univ. Math. J. 45 (1996) 1095–1118.
[20] M.C. Concordel, Periodic homogenization of Hamilton–Jacobi equations. II. Eikonal equations, Proc. Roy. Soc. Edinburgh A 127 (1997) 665–689.
[21] J.N.L. Connor, T. Uzer, R.A. Marcus, Eigenvalues of the Schrödinger equation for a periodic potential with nonperiodic boundary conditions; a uniform semiclassical analysis, J. Chem. Phys. 80 (10) (1984) 5095–5106.
[22] M. Crandall, P.L. Lions, Viscosity solutions of Hamilton–Jacobi equations, Trans. Am. Math. Soc. 282 (1984) 487–502.
[23] B. Engquist, O. Runborg, A.K. Tornberg, High frequency wave propagation by the segment projection method, J. Comput. Phys. 178 (2002) 373–390.
[24] L.C. Evans, Effective Hamiltonians and quantum states, Séminaire X-EDP 2000–2001. Available from <http://math.polytechnique.fr/seminaires/seminaires-edp/2000-2001/evans.ps>.
[25] L.C. Evans, D. Gomes, Effective Hamiltonians and averaging for Hamiltonian dynamics, I, Arch. Rational Mech. Anal. 157 (2001) 1–33.
[26] E. Fatemi, B. Engquist, S. Osher, Numerical solution of the high frequency asymptotic expansion for the scalar wave equation, J. Comput. Phys. 120 (1995) 145–155.
[27] P. Gérard, P.A. Markowich, N.J. Mauser, F. Poupaud, Homogenization limits and Wigner transforms, Commun. Pure Appl. Math. 50 (4) (1997) 323–379.
[28] P. Goatin, Oleinik estimates and uniqueness for hyperbolic systems of balance laws, Math. Models Meth. Appl. Sci. 13 (2003) 527–543.
[29] P. Goatin, L. Gosse, Decay of positive waves for $n \times n$ hyperbolic systems of balance laws, Proc. Amer. Math. Soc. (to appear).
[30] L. Gosse, Using K-branch entropy solutions for multivalued geometric optics computations, J. Comput. Phys. 180 (2002) 155–182.
[31] L. Gosse, F. James, Convergence results for an inhomogeneous system arising in various high frequency approximations, Math. 90 (2002) 721–753.
[32] L. Gosse, S. Jin, X. Li, Two moment systems for computing multiphase semiclassical limits of the Schrödinger equation, Math. http://dx.doi.org/10.1142/S0218202503003082.
[33] J.C. Guillot, J. Ralston, E. Trubowitz, Semiclassical asymptotics in solid-state physics, Commun. Math. Phys. 116 (1988) 401–415.
[34] F. Hövermann, H. Spohn, S. Teufel, Semiclassical limit for the Schrödinger equation for a short scale periodic potential, Commun. Math. Phys. 215 (2001) 609–629.
[35] S. Izumiya, G.T. Kossioris, Geometric singularities for solutions of single conservation laws, Arch. Rational Mech. Anal. 139 (1997) 255–290.
[36] S. Jin, X. Li, Multi-phase computations of the semiclassical limit of the Schrödinger equation and related problems: Whitham vs. Wigner, Physica D 182 (2003) 46–85.

[37] S. Jin, S. Osher, A level set method for the computation of multivalued solutions to quasi-linear hyperbolic PDEs and Hamilton–Jacobi equations, Commun. Math. Sci. 1 (3) (2003) 575–591.
[38] J.B. Keller, Semiclassical mechanics, SIAM Rev. 27 (1985) 485–504.
[39] H.J. Korsch, M. Glück, Computing quantum eigenvalues made easy, Eur. J. Phys. 23 (2002) 413.
[40] R. Kronig, W.G. Penney, Quantum mechanics of electrons in crystal lattices, Proc. R. Soc. A 144 (1931) 101.
[41] P.L. Lions, G. Papanicolaou, S.R.S. Varadhan, Homogenization of Hamilton–Jacobi equations, unpublished manuscript, circa 1988.
[42] P.L. Lions, T. Paul, Sur les measures de Wigner, Revista Mat. Iberoamericana 9 (1993) 553–618.
[43] P.L. Lions, B. Perthame, E. Tadmor, A kinetic formulation of multidimensional scalar conservation laws and related equations, J. Am. Math. Soc. 7 (1994) 169–191.
[44] P.L. Lions, B. Perthame, E. Tadmor, Kinetic formulation of the isentropic gas dynamics and p-systems, Commun. Math. Phys. 163 (1994) 415–431.
[45] D. Ludwig, Uniform expansions at a caustic, Commun. Pure Appl. Math. 19 (1966) 215–250.
[46] P. Markowich, N.J. Mauser, F. Poupaud, A Wigner-function approach to semiclassical limits: electrons in a periodic potential, J. Math. Phys. 35 (1994) 1066–1094.
[47] F. Poupaud, C. Ringhofer, Semi-classical limits in a crystal with external potentials and effective mass theorems, Commun. Partial Differential Equations 21 (1996) 1897–1918.
[48] O. Runborg, Some new results in multiphase geometrical optics, Math. Mod. Numer. Anal. 34 (2000) 1203–1231.
[49] C. Sparber, P. Markowich, N. Mauser, Multivalued geometrical optics: Wigner functions vs. WKB methods, Asymptotic Anal. 33 (2003) 153–187.
[50] W.W. Symes, J. Qian, A slowness matching Eulerian method for multivalued solutions of Eikonal equations, J. Sci. Comp. 19 (2003) 501–526.
[51] E. Tadmor, T. Tassa, On piecewise regularity of entropy solutions to scalar conservation laws, Commun. PDE 18 (1993) 1631–1652.
[52] A. Vasseur, Convergence of a semi-discrete kinetic scheme for the system of isentropic gas dynamics with $\gamma = 3$, Indiana Univ. Math. J. 48 (1999) 347–364.
[53] A. Zettl, Spectral theory and computational methods for Sturm–Liouville problems, in: D. Hinton, P.W. Schaefer (Eds.), Lecture Notes in Pure and Applied Mathematics, vol. 191, Marcel Dekker, New York, 1997.